Theory of extremal dynamics with quenched disorder: Invasion percolation and related models

R. Cafiero,[1] A. Gabrielli,[1] M. Marsili,[2] and L. Pietronero[1]
[1]*Dipartimento di Fisica, Universitá di Roma ''La Sapienza,'' Piazzale Aldo Moro 2, I-00185 Romá, Italy and Istituto Nazionale di Fisica della Materia, unitá di Roma I, Roma, Italy*
[2]*Department of Theoretical Physics, University of Manchester, Manchester M13 9PL, United Kingdom*
(Received 28 December 1995)

The study of phenomena such as capillary displacement in porous media, fracture propagation, and interface dynamics in quenched random media has attracted a great deal of interest in the last few years. This class of problems does not seem to be treatable with the standard theoretical methods, and the only analytical results come from scaling theory or mapping, for some of their properties, to other solvable models. In this paper a recently proposed approach to problems with extremal dynamics in quenched disordered media, named run time statistics (RTS) or quenched-stochastic transformation, is described in detail. This method allows us to map a quenched dynamics such as invasion percolation onto a stochastic annealed process with cognitive memory. By combining RTS with the fixed scale transformation approach, we develop a general and systematic theoretical method to compute analytically the critical exponents of invasion percolation, with and without trapping, and directed invasion percolation. In addition we can also understand and describe quantitatively the self-organized nature of the process. [S1063-651X(96)07207-8]

PACS number(s): 02.50.−r, 05.40.+j, 05.90.+m

INTRODUCTION

The study of extremal dynamical processes with quenched disorder has attracted great interest in the past few years. A wide range of phenomena, such as fluid displacement in porous media [1], fracture propagation or dielectric breakdown in disordered lattices [2,3], models for punctuated biological evolution [4], and interface dynamics in quenched disorder [5] can be described by dynamical models which select at each time step the extremal value of a quenched random field $\epsilon(x)$ plus, eventually, additional conditions, for example, a critical slope in interface dynamics [5]. The main characteristics of these models are (1) given a realization of the disorder, the dynamics is deterministic; (2) the dynamics is intrinsically critical, or self-organized, giving rise spontaneously to self-similar or self-affine structures, without any fine tuning of some parameter.

The paradigm of quenched extremal dynamics is invasion percolation (IP), a model which describes the quasistatic capillary displacement of a fluid in a porous medium. In IP, to each point of a discretized lattice is assigned a random variable, whose value is extracted from a flat probability density. Then, one chooses a seed point from which the dynamics starts. At the first time step the nearest neighbor of the seed with the smallest variable is chosen and added to the invading cluster (extremal dynamics). New variables are added to the perimeter of the cluster, and so on.

Irreversible dynamical models with quenched random variables, such as IP, cannot be addressed by the fixed scale transformation method [6,7] or by any other microscopic theory. Recently a general method to deal with quenched extremal dynamics has been proposed, called run time statistics (RTS) [8], or quenched-stochastic transformation, along with ideas introduced in Ref. [9] by Pietronero and Schneider, in a preliminary attempt to apply the fixed scale transformation (FST) approach to IP [6,9], and then deepened and extended to a wider field of applications by Marsili [8].

This method is based on the idea that a deterministic extremal dynamics such as IP can be mapped onto a stochastic dynamics with cognitive memory. When the IP dynamics starts, one does not know anything about the values of the quenched variables involved in the process, except that they have been extracted from a flat distribution. As soon as the extremal dynamics finds the smallest perimeter variable, one acquires additional information: all other perimeter variables are greater than the smallest one. This conditional information can be thought of as a cognitive memory, which *remembers* the past growth history. The quenched-stochastic transformation assigns to each perimeter variable a time-dependent probability density, whose evolution is determined by the extremal dynamics. The evolution of these *effective densities* depends on how many times a given variable i participated in the dynamics without being the smallest one, that is to say on the age W of the variable. An *old* variable will have a density more and more concentrated on great values, in that it lost many times in the competition with the other perimeter variables. By using these effective densities we are able to map the extremal IP dynamics onto an annealed stochastic process, where each variable is assigned a growth probability (the probability to be the smallest one), which decays to zero as the *age* of the variable tends to infinity.

The RTS method allows us to develop a comprehensive and systematic theoretical scheme for extremal dynamics (the RTS-FST approach), whose essential points follow.

(1) Quenched-stochastic transformation.

(2) Identification of the microscopic asymptotic dynamics. This point clarifies the self-organized critical (SOC) nature of the problem.

(3) Identification of the scale-invariant dynamics for block variables. This point elucidates the nature of scale invariance in the problem.

(4) Definition of the stochastic scale-invariant local growth rules corresponding to the mapping of the original problem. This clarifies the origin of avalanche dynamics.

(5) Use of the above elements in the FST scheme to compute analytically the independent exponents.

This project has already been carried out successfully to describe the self-organized critical state of the Bak and Sneppen model [4] via a real space renormalization-group (RG) approach [10].

In this paper, after a detailed discussion of RTS theory, the RTS-FST approach is developed to compute analytically the fractal dimension of invasion percolation with and without trapping and of directed invasion percolation (DIP). The avalanche size distribution of IP at the fixed point is also investigated and the critical exponent τ is computed, using the RTS approach. All the analytical results we derive are in very good agreement with numerical simulations and scaling arguments [1,11,12].

In particular, in Sec. I we introduce the IP model and describe the RTS theory, its essential concepts as well as its detailed mathematical formulation. The derivation is illustrated by simple examples. We shall stress the relations between a quenched process based on extreme statistics and a stochastic process. This will enable us to understand properly in which sense the stochastic process of the RTS corresponds to the quenched process.

In Sec. II we first review the phenomenology of invasion percolation and related models. We stress how the RTS captures the essential features which emerge from this picture. These are mainly related to the memory effects which arise in its dynamics. Memory provides the main mechanism for both self-organization and the generation of fractal structures. Then we develop the RTS-FST approach for IP, with and without trapping and DIP. Special attention is devoted to the identification of the scale-invariant dynamics of IP and to the implementation of the infinite time limit (freezing condition for fractals), the fundamental ingredients of the FST approach, which needs a different implementation for extremal dynamics with respect to other stochastic growth processes [6].

In Sec. III we compute analytically the exponent of the size distribution of critical avalanches for IP. Our result is in very good agreement with numerical simulations.

In the final section we summarize the main result and discuss possible extensions of the methods developed in this work.

I. EXTREMAL DYNAMICS AND STOCHASTIC PROCESSES

A. Model and formalism

As a model for quenched dynamics with extremal statistics, we will consider invasion percolation. The model is defined as follows. To each bond of a discretized lattice is associated a random variable ϵ_i with flat probability density $p(x)=1$. Without loss of generality one can define the ϵ_i in the range $[0,1]$. The dynamics evolves by occupying the bonds of the lattice. The values of the random variables ϵ_i are extracted from the $p(x)$ before the dynamics starts. At time $t=0$ one seed bond i_0 is chosen, from which the invasion process starts. Then, at time $t=1$, the nearest neighbor

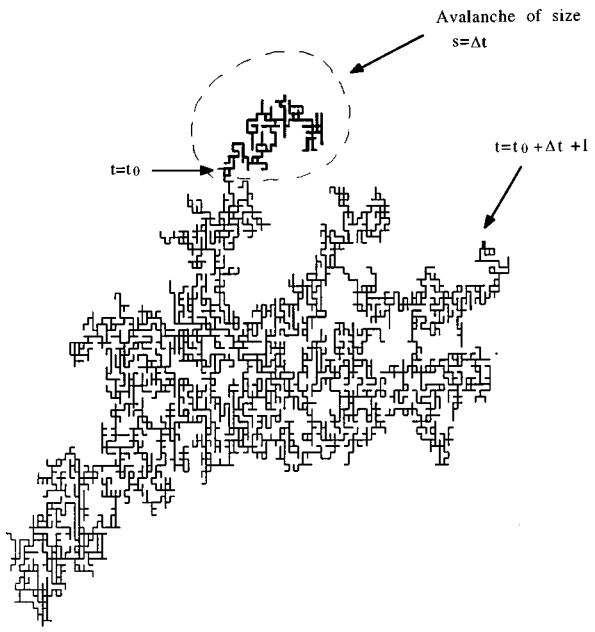

FIG. 1. The dynamics of invasion percolation consists of local macroevents, the avalanches, which are sequences of elementary events causally and spatially connected. In the figure, an avalanche (that surrounded by a dotted line) starts at time t_0 and evolves for a time s. At time t_0+s+1 the activity is transferred to another region of the cluster (the thick bond in the figure).

of i_0 with the smallest random variable, i_1, is added to the cluster $\mathcal{C}_{t=1}$, and its nearest neighbors are added to the perimeter $\partial\mathcal{C}_{t=1}$. At the next step the bond with the smallest random variable among the perimeter $\partial\mathcal{C}_{t=1}$ of the cluster is selected and added to the cluster, and so on. At any time step the variables ϵ_i on the perimeter are tested to find the smallest one. The main characteristics of this model follow.

(1) The dynamics, given a realization of the disorder and the seed bond i_0, is *deterministic*.

(2) *Self-organization*. The process spontaneously develops a scale-invariant structure with critical properties. In the limit $t\to\infty$ both long range space and time correlations appear.

(3) *Avalanches*. the asymptotic dynamical evolution consists of local macroevents, composed by elementary growth steps casually and spatially connected, called avalanches. When an avalanche stops, the activity is transferred to another region of the perimeter, leaving a structure with the fractal properties of the infinite percolating cluster (see Fig. 1). Avalanches show scale-invariant size distribution, as a consequence of long range temporal correlations in the dynamics.

This model, which describes the dynamics of invasion percolation, can be easily generalized to other extremal models [8], such as the Bak and Sneppen model [4] or the Sneppen model for quenched surfaces [5].

B. The quenched-stochastic transformation

In the transformation of the quenched dynamics into a stochastic one, an essential requirement is that the statistical weights of the realizations of the quenched process are correctly reproduced by the corresponding annealed stochastic

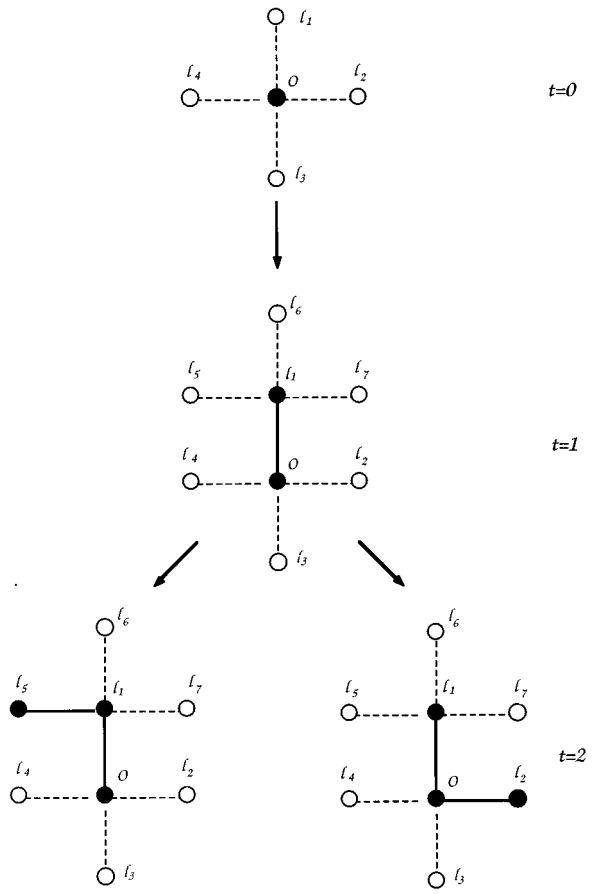

FIG. 2. Scheme for the calculation, with the exact method, of the weight of paths of length 2.

dynamics. It is therefore worthwhile to analyze in some detail how one can evaluate the probability of a realization, or ''path,'' of the IP dynamics. A rigorous way to do this is to impose all the order relations between the random variables of the bonds compatible with the growth history of the path and then to average simultaneously over all the realizations of the random variables. The probability W_q of the path will be

$$W_q = \int d\epsilon_{j_1} p_{0,0}(\epsilon_{j_1}) \cdots \int d\epsilon_{j_l} p_{0,0}(\epsilon_{j_l}) f(\epsilon_{j_1}, \ldots, \epsilon_{j_l}), \tag{1}$$

where $\{j_1, \ldots, j_l\}$ are the bonds participating in the formation of the path, $p_{0,0}(x)$ is the probability density of the variables ϵ_i, and $f(\,)$ is a combination of step functions $\theta(\epsilon_i - \epsilon_j)$ which implement all the possible order relations $\epsilon_i > \epsilon_j$ between the variables. Let us compute, for example, the weight of the paths of length 2 shown in Fig. 2, for a model with ''site'' growth rule, with $\mathcal{C}_0$ being the site O, $\partial\mathcal{C}_0$ being the four nearest neighbors of O, $\{l_1, l_2, l_3, l_4\}$, and with density $p_{0,0}(x) = 1$.

At time $t = 1$ we let the site l_1 grow and after this the sites $\{l_5, l_6, l_7\}$ enter the perimeter $\partial\mathcal{C}_1$ (Fig. 2).

At time $t = 2$ there are 2 possibilities: (1) growth of one new site between $\{l_5, l_6, l_7\}$; and (2) growth of one old site (frustrated one time) between $\{l_2, l_3, l_4\}$. Now we compute the probabilities of paths (1) and (2).

(1) At $t = 2$ the site l_5 grows. The two allowed order relations are (a) $\epsilon_{l_1} < \epsilon_{l_5} < \epsilon_{l_i}$ where $i = 2,3,4,6,7$; and (b) $\epsilon_{l_5} < \epsilon_{l_1} < \epsilon_{l_j}$ where $j = 2,3,4$ and simultaneously $\epsilon_{l_5} < \epsilon_{l_k}$ with $k = 6,7$. The probability P_1 of the path is

$$P_1 = \int_0^1 d\epsilon_{l_1} \int_{\epsilon_{l_1}}^1 d\epsilon_{l_5} (1 - \epsilon_{l_5})^5 + \int_0^1 d\epsilon_{l_5} (1 - \epsilon_{l_5})^2 \times \int_{\epsilon_{l_5}}^1 d\epsilon_{l_1} (1 - \epsilon_{l_1})^3 = \frac{5}{84} \simeq 0.0595. \tag{2}$$

(2) At time $t = 2$ the site l_2 grows. This can occur if $\epsilon_{l_1} < \epsilon_{l_2} < \epsilon_{l_i}$ where $i = 3,4,5,6,7$, leading to the following expression for the probability P_2:

$$P_2 = \int_0^1 d\epsilon_{l_1} \int_{\epsilon_{l_1}}^1 d\epsilon_{l_2} (1 - \epsilon_{l_2})^5 = \tfrac{1}{42} \simeq 0.0238. \tag{3}$$

Let us now switch to a generic stochastic process. This is based on the following elements: (a) a set of time-dependent dynamical variables $\{\eta_{i,t}\}$ for each bond i of the lattice; (b) a growth probability distribution (GPD) for the single growth step $\{\nu_{i,t}\}$, obtained from the $\{\eta_{i,t}\}$ and their time evolution rule; and (c) a rule for the evolution of the dynamical variables $\eta_{i,t} \to \eta_{i,t+1}$. For such a stochastic process, the statistical weight of a realization of t steps of the dynamics is just

$$W_s(t) = \prod_{n=1}^{t} \nu_{i(n),n}, \tag{4}$$

where $i(n)$ is the site selected by the dynamics at time n.

Therefore in order to map IP onto a stochastic process we have to (a) find the correct dynamical variables (the $\eta_{i,t}$'s); (b) determine the GPD $\{\nu_{i,t}\}$ in terms of these variables; and (c) find the rule by which the dynamical variables are updated. This is exactly the program carried out by the RTS theory.

We can get an insight into the essence of the question by analyzing the simplest possible process. We start with two independent random variables X_1, X_2 uniformly distributed in $[0,1]$ and we eliminate the smallest, for example, X_2. Clearly the probability that $X_1 > X_2$ is 1/2. Then, we compare the surviving variable X_1 with a third, uniform, random variable X_3 and, again, we eliminate the smallest one. At first sight one could say that, as before, since both variables are uniform, the probability that X_1 survives again is 1/2. A more careful calculation reveals that this expectation is wrong. In this case we indeed need to evaluate the probability that $X_1 > X_3$ given that $X_1 > X_2$. This, using the rules of conditional probability, reads

$$\widetilde{P}(X_1 > X_3) = P(X_1 > X_3 | X_1 > X_2) = \frac{P(X_1 > X_3 \cap X_1 > X_2)}{P(X_1 > X_2)} = \tfrac{2}{3}, \tag{5}$$

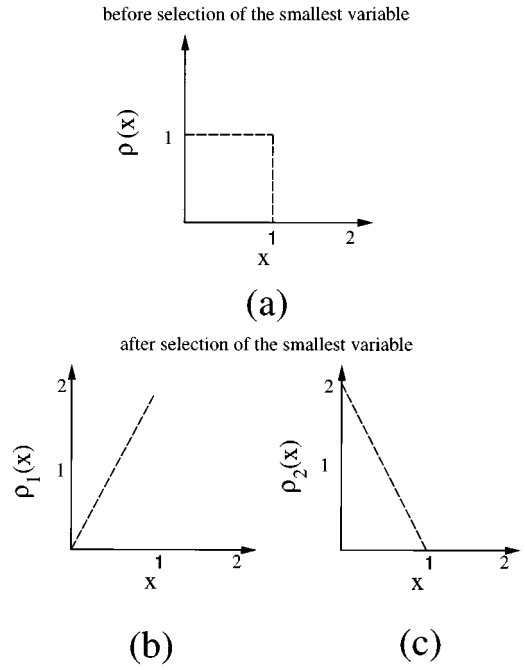

FIG. 3. Conditional evolution of the effective densities for the two-variable case. (a) The density of variables X_1 and X_2, before the selection of the smallest one is uniform. (b) Density of X_1 after one step of the extremal dynamics. (c) Density of X_2 after one step of extremal dynamics.

where we used the notation $P(A|B)$ for the probability of the event A given that B occurred and $P(A\cap B)$ for the probability of occurrence of both A and B. The problem with our ''first sight'' argument is that the variable X_1 is no *longer* uniform when it is compared with X_3. The information $X_1>X_2$ changes in a conditional way the probability density of X_1. Indeed the probability $\rho_1(x)dx$ that $x\leqslant X_1<x+dx$ must now account for the fact that $X_2<x$. Since $P(X_2<x)=x$ for a uniform variable, a trivial calculation yields $\rho_1(x)=2x$ (Fig. 3). Note that with this distribution of X_1 one can correctly calculate the probability $P(X_1>X_3)=2/3$ as given in Eq. (5). On the same footing, one can verify that also the distribution of X_2 is no longer uniform, but it is $\rho_2(x)=2(1-x)$ (Fig. 3). Qualitatively, the event $X_1>X_2$ decreases the probability that X_1 has small values. On the contrary, the probability that X_2 is small is enhanced.

The IP process can be thought of as a generalization of the above simple process, to the case where more than two variables participate in the selection and elimination of the smallest one. Loosely speaking, a variable ϵ_i experiences a frustration each time another variable ϵ_j is found to be smaller than it. The message of the above example is that this frustration is recorded in the distribution of the variable ϵ_i. As a result of repeated comparisons, the distribution of the variables on the interface evolves in time. These distributions $\rho_{i,t}(x)$, which we label with the bond index i and the time t, can therefore be taken as the dynamical variables of the stochastic process we are looking for, and will be referred to as the run time statistics. The RTS $\rho_{i,t}(x)$ changes from time t to time $t+1$ only for bonds which are in $\partial\mathcal{C}_t$. Indeed the minimum potential is chosen among the ϵ_i for $i\in\partial\mathcal{C}_t$. Bonds which are not in the cluster $\mathcal{C}_t$ or in $\partial\mathcal{C}_t$ will maintain their original distribution $\rho_{i,t}(x)=p_{0,0}(x)$. The evolution of the RTS $\rho_{i,t}(x)$ will start at the time t_0 when it first enters the set of perimeter bonds $\partial\mathcal{C}_{t_0}$, and will stop only when, if ever, at time t_1 the bond i will be selected being the one with the minimum variable among those in the perimeter $\partial\mathcal{C}_{t_1}$. Indeed, for $t>t_1$ the bond will belong to the cluster $\mathcal{C}_t$, and the process will not gain any more information on the statistics of the variable ϵ_i.

Therefore the distribution of ϵ_i at time $t\in[t_0,t_1)$ will depend only on the number of times $k=t-t_0$ it has not been selected, or equivalently on the ''age'' k of the bond i, which is the time it has spent in the perimeter. More precisely, bonds that have been in the perimeter for the same number k of temporal steps have the same dynamical history and will have the same RTS, independently of their location on the perimeter. This motivates the introduction of an alternative notation for the RTS and for the GPD in terms of the index k:

$$\rho_{i,t}(x)\equiv p_{k,t}(x) \text{ and } \quad \nu_{i,t}\equiv\mu_{k,t}$$

$$\forall i\in\cap_{m=t-k}^{t}\partial\mathcal{C}_m\cap\overline{\partial\mathcal{C}}_{t-k-1}, \tag{6}$$

where $\overline{\partial\mathcal{C}_t}$ indicates the complement of $\partial\mathcal{C}_t$, the entire lattice minus the interface, and the set in Eq. (6) contains the bonds with age k, those entered in the perimeter at time $t-k$ and which still belong to the perimeter at time t. Furthermore, we shall define $n_{k,t}$ as the number of perimeter bonds that have been on it for k temporal steps. The sum of $n_{k,t}$ over k gives the total number of perimeter bonds at time t: $\Sigma_k n_{k,t}=N_t=|\partial\mathcal{C}_t|$.

Having defined the RTS $\rho_{i,t}(x)$ as our dynamical variables, we are now in a position to evaluate the growth probability distribution. Again this amounts to a generalization of the above simple example, where it was shown that the probability that $X_1>X_3$ could be evaluated correctly in terms of the updated distribution of X_1. Indeed, assuming the RTS $\rho_{i,t}(x)$ are known for all $i\in\partial\mathcal{C}_t$, we can evaluate the probability that the dynamics of IP will select the site i. This is indeed, if the site i has been tested k times, just $\mu_{k,t}=\nu_{i,t}=P(\epsilon_i=\min_{m\in\partial\mathcal{C}_t}\epsilon_m)$, which reads (see Appendix A for details)

$$\mu_{k,t}=\int_0^1 dx\; p_{k,t}(x)\prod_{\theta}\;[1-P_{\theta,t}(x)]^{n_{\theta,t}-\delta_{\theta,k}}, \tag{7}$$

where $P_{\theta,t}(x)=\int_0^x p_{\theta,t}(y)dy$. The $\{\mu_{k,t}\}$ is the GPD of the stochastic process corresponding to our quenched dynamics. This is correctly normalized, as can be explicitly checked [8], and Eq. (7) is an exact relation. The selection of one bond i with this GPD has the same effects, which were discussed for our simple example, on the distribution of the variable ϵ_i which has been selected and on those of the bonds j which remain on the perimeter set. The generalization of our simple example is carried out in detail in Appendix A using the rules of conditional probability. In practice, however, this procedure may require some approximations, because, depending on the specific problem, certain space correlations between variables may be neglected, in order to

define the stochastic process as sequential [13]. We are going to discuss this point in more detail later on. The result is that the density $m_{k,t}(x)$ of the grown bond i can be written as

$$m_{k,t}(x)=\frac{p_{k,t}(x)\prod_{\theta}[1-P_{\theta,t}(x)]^{n_{\theta,t}-\delta_{\theta,k}}}{\mu_{k,t}}, \tag{8}$$

while the density of a perimeter bond with age k at time t becomes

$$p_{\theta+1,t+1}(x)=p_{\theta,t}(x)\int_0^x \frac{m_{k,t}(y)}{1-P_{\theta,t}(y)}dy. \tag{9}$$

Equations (7)–(9) give the conditional evolution of the effective densities of the perimeter variables.

At this point, we can analyze the situation at time $t+1$, after the growth at time t. The bond i is added to the cluster; its RTS does not evolve anymore. We have seen how the RTS of the ''surviving'' perimeter bonds evolves. Then, $n_{0,t+1}$ bonds with density $p_{0,t+1}(x)=p_{0,0}(x)$ enter in the perimeter $\partial\mathcal{C}_{t+1}$. The time evolution of $n_{\theta,t}$ for $\theta\neq 0$ is given, for IP, by

$$n_{\theta+1,t+1}=n_{\theta,t}-\delta_{k,\theta}. \tag{10}$$

In summary, given the dynamical variables $p_{k,t}(x)$ at time t, we can compute the transition probabilities from a configuration of IP at time t to all the accessible configurations at time $t+1$ by Eq. (7). Using Eqs. (8) and (9) we can update the dynamical variables and find $p_{k,t+1}(x)$. We can repeat the same procedure for the next time step, and so on for any subsequent step. So, Eqs. (7)–(9) accomplish our goal of describing a quenched process, based on extremal dynamics, as a stochastic process with cognitive memory.

The use of the interval $[0,1]$ or the choice of uniform initial probability density $p_{0,0}(x)=1$ does not influence the geometrical and dynamical properties of the growth process. This results from the invariance of the above equations under the transformation $\int_0^x dy\, p_{0,0}(y)\to x$ that maps a general density $p_{0,0}(x)$ onto the uniform one.

It is instructive at this point to use the RTS in order to compute the weights of the ordered paths of Fig. 2. A comparison with the exact results of Eqs. (2) and (3) yields indeed a direct test of the validity of the RTS and of its approximation scheme. Using the RTS, P_1 and P_2 are the product of the probabilities of the single step events composing the path. For the first path (Fig. 2), $P_1=\nu_{l_1,t=1}\nu_{l_5,t=2}$ where $\nu_{l_1,t=1}$ is evaluated by observing that $\rho_{l_i,0}(x)\equiv p_{0,0}(x)\equiv 1$ with $i=1,2,3,4$, and applying Eq. (7):

$$\nu_{l_1,t=1}=\int_0^1 d\varepsilon_{l_1}(1-\varepsilon_{l_1})^3=\tfrac{1}{4}.$$

In order to find the probability of the second step we need to update the RTS of l_2,l_3,l_4 using Eqs. (8) and (9):

$$\rho_{l_i,t=1}(x)\equiv p_{1,1}(x)=\tfrac{4}{3}[1-(1-x)^3],\quad i=2,3,4$$

while the new sites l_5,l_6,l_7 have density $p_{0,0}(x)$. Using again Eq. (7) we find

$$\nu_{l_5,t=2}=\int_0^1 d\varepsilon_{l_5}\left(\int_{\varepsilon_{l_5}}^1 dx\right)^2\left[\int_{\varepsilon_{l_5}}^1 dx\,\tfrac{4}{3}[1-(1-x)^3]\right]^3=\tfrac{94}{405},$$

which therefore yields

$$P_1=\nu_{l_1,t=1}\nu_{l_5,t=2}=\tfrac{47}{810}\simeq 0.0580.$$

An analogous calculation for $P_2=\nu_{l_1,t=1}\nu_{l_2,t=2}$ gives

$$P_2=\tfrac{41}{1620}\simeq 0.0253.$$

Comparing these with the exact results, $P_1\simeq 0.0595$ and $P_2\simeq 0.0238$, we find a small discrepancy. In spite of the care paid to account for all the statistical information stored by the process, using diligently the rules of conditional probability, we cannot recover the exact result for a path of only two steps. The roots of this discrepancy can be traced back to the very beginning of our discussion and lie in the very definition of quenched and stochastic processes [13]. Note, however, that if one had more variables than just two the discrepancy would be much smaller. The present example is a single one in which this effect is enhanced.

Let us have a closer look at Eqs. (1) and (4). When Eq. (4) is used with the RTS to evaluate the probability of a path, we discover two main differences.

(1) First of all W_q in Eq. (1) does not have the form of a product. The integrals in Eq. (1) cannot be factorized into a product of single step transition probabilities. This is clearly evident in Eqs. (2) and (3) already for a path of two steps. This means that *it is not possible, in general, to map exactly a quenched extremal dynamics into a sequential stochastic dynamics*.

(2) Each disorder variable ϵ_i is integrated only once in W_q. On the contrary, Eq. (7) implies that each variable is integrated over at each time step of which it partakes. Therefore the expression of W_s resulting from Eq. (4), would contain many integrals on the same disorder variable ϵ_i. This suggests that in the RTS process the disorder variables are not fixed as in the quenched process. The variables involved in the dynamics, those on perimeter bonds, are replaced at each time step by new variables with different statistical properties. This procedure captures the essential features of the original dynamics with quenched variables. Its practical implementation requires certain technical approximations which, however, can be quantitatively controlled [14]. Strictly speaking it is not possible to obtain a sequential stochastic process by integrating over all variables at each time step. The RTS provides the sequential stochastic process which best approximates the quenched dynamics. We have reasons to believe that the *intrinsic* approximations contained in the RTS improve when the system size becomes larger, and vanishes in the thermodynamic limit [14,13]. Even though at the moment we have no definite proof of this, we note that the successes [8,10] reported by the RTS in correctly describing the properties of extremal dynamics processes, including those to be derived in the rest of this paper, strongly support this belief.

We shall return later to the qualitative features which emerge from the RTS dynamics; for the time being let us summarize the dynamical rules of the RTS process for IP. The lattice bonds can be grouped in three classes.

(1) *Bonds being in* $\partial\mathcal{C}_t$; they have density $\rho_{i,t}(x)=p_{k,t}(x)$ and we call them *active bonds*.

(2) *Bonds being in* $\mathcal{C}_t$; they have density $\rho_{i,t}(x)=m_{k_{t_0},t_0}(x)$, where t_0 is the time at which they have grown. We call these *idle bonds*, because after the growth their density no longer evolves and it does not influence the evolution of the RTS of the *active bonds*.

(3) *Bonds that are neither in* $\mathcal{C}_t$ *nor in* $\partial\mathcal{C}_t$; they have density $\rho_{i,t}(x)=p_{0,0}(x)$, because they have not participated in the dynamics up to time t. We call them *neutral bonds*.

During the dynamical evolution, the following transitions will take place:

$$neutral \rightarrow active,$$

$$active \rightarrow idle.$$

We now proceed to discuss a specific example.

II. APPLICATION OF THE RTS TO THE STUDY OF IP AND DIP

A. Percolation and invasion percolation

We briefly introduce the characteristics of the ''static'' percolation, as described, for example, in [15]. Let us consider a d-dimensional lattice, say a cubic one. We associate to each bond (or site) i of the lattice, independently from each other, a random number $\epsilon_i \in [0,1]$ extracted with uniform probability density $p(x)=1$. Then, we choose a threshold value p and introduce this occupation rule: the bonds with $\epsilon_i < p$ are occupied, and the others remain unoccupied. In this way, each bond will be occupied with probability p and not occupied with probability $(1-p)$. We say that the structure composed by the occupied bonds percolates if it contains as a connected structure that spans the lattice in all directions. An important property of this model is that there is a critical value $p_c<1$, for $d>1$, depending on the lattice coordination number and on the dimension d, such that for $p>p_c$ one has a percolating cluster and for $p<p_c$ it does not exist. One can show that the percolation model exhibits at p_c a typical second order phase transition with one relevant parameter p and a repulsive fixed point at p_c. Near this fixed point the relevant quantities of the model show power law behavior with critical scaling exponents [15]. The existence of an upper critical dimension $d_c=6$ allows us to use renormalization-group methods together with the ϵ expansion to calculate these exponents.

Let us concentrate on the geometrical properties of the percolating cluster for two-dimensional (2D) bond percolation. For $p<p_c=1/2$ there is no percolating cluster, as we said before. For $p>p_c=1/2$ the percolating cluster is compact with $D_f=2$ and there are other finite clusters up to a given size. For $p=p_c=1/2$ there is an intermediate behavior: the percolating cluster is fractal with $D_f=\frac{91}{48}\simeq 1.8956$ and there are many other finite clusters of all dimensions, without a characteristic size. The probability distribution of the cluster size follows the scaling relation:

$$P(s;p)=sn(s;p)=s^{-\tau}f[|p-p_c|s^{\sigma}], \tag{11}$$

where $n(s;p)$ is the mean number of clusters of size s per bond, $1<\tau<2$, and $\sigma>0$ is associated to a cutoff size $s_0=|p-p_c|^{-1/\sigma}$. This scaling relation becomes, at p_c,

$$P(s;p_c)\propto \frac{1}{s^{\tau}}.$$

For 2D bond percolation exact methods [15] give $\tau=96/91$. In Sec. III an analogous characteristic quantity of IP, the avalanche distribution, will be studied both analytically and numerically.

The invasion percolation model with its variations (IP with trapping and directed IP) is the main subject of this paper. It was introduced in 1980 [17], and it is really interesting for the following reasons.

(1) It can be used, as in the original applications [1,16,17], to describe the active displacement (the dynamics) of a fluid in disordered media by another unmixable fluid, under an external or internal pressure.

(2) IP seems to reproduce, as we will explain further on, in a *self-organized* way, the geometrical properties of the percolating cluster. This is a particularly interesting situation because the same geometric entity arises from both an usual critical behavior and a self-organized one.

(3) IP can be considered as the paradigm of all quenched growth dynamics with extremal statistics.

The main application of IP is to the phenomenon of fluid displacement of a *defender* fluid in a porous medium by another fluid, the *invader*, unmixable with the defender, when capillarity forces prevail. The medium is often modeled as a hydraulic network of throats and pores. Here we represent it as a bidimensional lattice where the bonds represent the throats and the sites represent the pores. To both sites and bonds is associated a random variable that reproduces the pore and throat size.

A fundamental phenomenological quantity is the capillary number C given by

$$C=\frac{\mu v}{\gamma},$$

where μ is the viscosity, v the mean speed, and γ the surface tension. It reproduces the ratio between viscous and capillary forces. The regime we are interested in is realized when $C \ll 1$. In this limit the invader occupies the bonds with the smallest size, that is to say, the greatest surface tension. If also $v \ll 1$, we are in the quasistatic regime, and the dynamics coincides with that of the IP model previously introduced. From the point of view of fluid displacement $\mathcal{C}_t$ is the inv ader and $\partial\mathcal{C}_t$ is the interface between the two fluids. The sites of the lattice that are extremes of a bond in $\mathcal{C}_t$ belong to the cluster, as usually happens for fluid displacement in porous media. The dynamics stops after the invader spans (percolates) the lattice.

In order to avoid finite size effects [16] we are interested in the case of a very large lattice; this allows us to consider the limits $r\rightarrow\infty$ and $t\rightarrow\infty$, for which the scale-invariant properties of the model are well defined. An interesting phenomenon occurring during fluid displacement is that of *trapping*. Trapping occurs when the defender is totally incompressible and a bubble of defender is completely surrounded

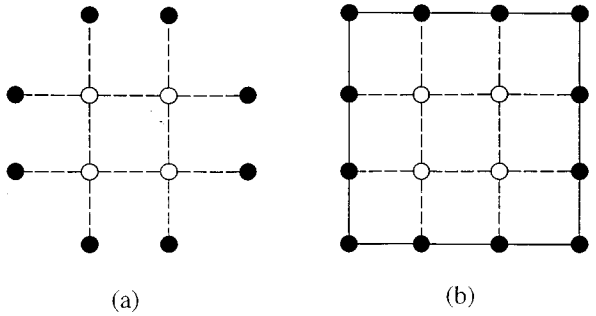

FIG. 4. (a) Trapping I or trapping per site; (b) trapping II or trapping per bond. ○ and the dotted segments indicate the defender (oil), while ● and filled segments are the invader (water). (b) is more rare than (a), because a configuration verifying (b) will verify (a) also, but the converse is not true.

by the invader: the invader will no longer invade the surrounded region. This effect creates extra holes in the invader cluster, lowering its fractal dimension. There are two possible definitions of trapping [11]. In order to understand them we need to introduce the concept of edge connectedness of a defender cluster to the lattice edges: *the defender cluster is connected if there is a path of defender bonds (and sites) connecting the cluster to the lattice edge*. The two definitions of trapping follow.

(1) *Trapping I* (site trapping): a cluster of defender bonds is trapped if it does not satisfy the edge connectedness condition [Fig. 4(a)].

(2) *Trapping II* (bond trapping): a cluster of defender bonds is trapped if it does not satisfy the edge connectedness condition and it is surrounded by a closed path of invader bonds [Fig. 4(b)].

Trapping I corresponds to usual trapping in fluid displacement. Moreover, trapping II is rare with respect to trapping I.

Most of the results obtained until now on IP with and without trapping, except some [18], derive from numerical analysis of large simulations of the process [11,12]. These results concern mainly IP without trapping because trapping is a nonlocal, very difficult to handle, effect.

Let us start from IP without trapping. It has been demonstrated that, in the limit of infinite lattice, the asymptotic properties of the percolating cluster do not depend on $\mathcal{C}_0$, provided that it is finite [18]. In [17,16] one defines a useful quantity, the acceptance profile $a_t(x)$, given by the ratio between the number of bonds in $\mathcal{C}_t$ with variable ranging between x and $x+dx$ and the total number of bonds with variable between x and $x+dx$ in $\mathcal{C}_t U \partial\mathcal{C}_t$. The function $a_t(x)$ has in the limit $t\to\infty$ the following behavior, obtained both by simulations and by rigorous demonstration [18]:

$$\lim_{t\to\infty} a_t(x) = \theta(p_c - x), \tag{12}$$

where p_c is the critical threshold of static percolation. Equation (12) means that, asymptotically, almost all the bonds in the perimeter with variable less than p_c will eventually grow, and almost all the bonds with variable larger than p_c will not grow. This is a proof of the correspondence between IP and static percolation at the critical point.

TABLE I. Fractal dimension vs order n for IP without trapping (D_f), with site trapping (D_f^{I}), with bond trapping (D_f^{II}), and for directed IP (D_f^{DIP}). In the last two lines we compare the FST results with known analytical and simulation values.

Order n	$D_f(n)$	$D_f^{\mathrm{I}}(n)$	$D_f^{\mathrm{II}}(n)$	$D_f^{\mathrm{DIP}}(n)$
3	1.7039	1.6965	1.7029	1.6254
4	1.7941	1.7378	1.7825	1.6626
5	1.8228	1.7506	1.8066	1.6924
6	1.8473	1.7599	1.8245	1.7081
7	1.8565	1.7642	1.8317	1.7189
8	1.8645	1.7678	1.8372	1.7250
9	1.8677	1.7697	—	—
⋮	⋮	⋮	⋮	⋮
∞	1.8879	1.7812	1.8544	1.7444
Analytical	$\frac{91}{48}\simeq 1.895$[a]			$\simeq 1.748$[b]
Simulation	∼1.89[1]	∼1.82[11]	∼1.86[11]	

[a]Conformal mapping applied to 2D Percolation [15].
[b]Series expansion [27].

Another rigorous result for IP is that the ratio between N_t and the cluster mass t tends to a constant different from zero [18]:

$$\lim_{t\to\infty} \frac{N_t}{t} = \frac{1-p_c}{p_c} \neq 0, \tag{13}$$

which depends on the critical threshold. The limit in Eq. (13) would vanish for any compact structure. Therefore Eq. (13) implies that the clusters generated by IP are fractal. Indeed, large scale simulations of IP [11] give $D_f^{\mathrm{IP}} \simeq 1.89$, which coincides, within numerical accuracy, with the fractal dimension of percolating clusters at $p = p_c$.

Finally it is seen that the dynamics of IP occurs in *sequential bursts of activity*, which can be thought of as macroevents called *avalanches*. An avalanche is a temporal consecutive set of growth events causally and spatially connected to a first growth event. The distribution of avalanche duration is therefore the same as the distribution of the total number of bonds s involved:

$$D(s) \sim s^{-\tau}, \tag{14}$$

which reflects the critical character of the dynamics. These results support the hypothesis [16] that IP asymptotically reproduces the geometrical properties of the infinite cluster of critical percolation.

The same picture applies to IP with trapping: the acceptance profile, though more slowly and asymmetrically with respect to p_c [1], tends asymptotically to Eq. 12. The surface to volume ratio, also, does not vanish, and the geometry of the clusters turns out to be described by a well defined value of the fractal dimension. Simulation results [11] give $D_f \simeq 1.82$ for site trapping, and $D_f \simeq 1.86$ for bond trapping (see Table I). Note that trapping effect, in both cases, adds empty zones to the growing structures leading to a fractal dimension lower than that of IP without trapping.

This general picture also emerges from an analysis of the RTS equations. The statistical properties of the active variables on the perimeter are described by the histogram

$\Phi_t(x)=\langle h_t(x)\rangle/\langle N_t\rangle$, where $h_t(x)$ is the histogram for a given realization of the disorder, N_t is the number of active variables at time t, and $\langle\ \rangle$ is the mean over all realizations of disorder. The $\Phi_t(x)$ function, apart from normalization, is the complement of the acceptance profile $a_t(x)$. Using the RTS equations one can write the following histogram equation for the time evolution of $\Phi_t(x)$ [8]:

$$\partial_x\Phi_t(x)=\beta\Omega_t\Phi_t^2(x)\left[1-\frac{\omega_t}{\omega_t+1}\Phi_t(x)\right], \tag{15}$$

where $\Omega_t=\langle N_t\rangle$, $\omega_t=\langle N_{t+1}-N_t\rangle$, and β is a function of Ω_t. The solution $\Phi_t(x)$ of this equation becomes asymptotically $\lim_{t\to\infty}\Phi_t(x)=[1/(1-\rho_c)]\theta(x-p_c)$, where p_c is the critical threshold of the original extremal dynamics. This clarifies the SOC nature of the problem. A similar equation describing the SOC behavior of extremal dynamical models, the gap equation, has been obtained by Bak *et al.* [4], based on phenomenological assumptions. Our histogram equation is instead derived directly from the microscopic dynamics.

The mechanism responsible for the formation of a fractal structure can also be readily appreciated. It is indeed known [17] that the feature of a growth dynamics which can produce a fractal structure is the presence of *screening* at all length scales. Let us borrow the dielectric breakdown model (DBM) [19] in order to illustrate this point. Here the Laplace equation conspires with the growing cluster in such a way that the probability of growth on a site drops exponentially to zero with its distance from the tips of the structure. This means that whole regions of the perimeter of the cluster can be considered, to a good approximation, as ''frozen,'' when the probability of the growth events in this region becomes very small. Furthermore, the screening effects act [17] at all length scales, as suggested by the scale invariance of the Laplace equation. Therefore the process leaves similar frozen structures at all length scales, i.e., it produces a fractal.

A crucial point in the practical translation of these observations is that a growth process produces a scale-invariant structure if and only if its dynamics can be described at all (large enough) length scales in the same way, i.e., if the process is characterized by a *scale-invariant dynamics*. Therefore, in order to understand a process which produces fractal structures, it is essential to find its scale-invariant dynamics [20,21,7]. We shall examine in detail the scale-invariant dynamics of IP in the forthcoming section. For the time being, we make some comments on the main qualitative feature which is responsible for the emergence of screening effects in the dynamics of IP and therefore of its fractal properties.

The effective screening arises in IP from the memory effects intrinsic in the dynamics. Qualitatively, we have seen that a bond on the perimeter which has not been selected for a long time (i.e., a bond with a RTS index, or age $k\gg 1$) will have very little chance of being selected. In other words, the probability $\mu_{k,t}$ decreases as the age k of the bond increases. This observation can be quantified by a crude approximation which reveals that $\mu_{k,t}\sim(k+1)^{-\alpha}$, the exponent being $\alpha=2$ within the approximation [8]. A numerical test of this relation confirms its behavior but results in a value of $\alpha=1.35\pm 0.05$ [22]. The lack of a characteristic time in this relation is at the very heart of scale invariance in IP (indeed, time and length scales are related by a power law $t\sim\ell^{D_f}$). However, the nature of screening here is quite different from that in the DBM model, where it was directly related to the geometry of the cluster. Here screening occurs in time, irrespective of space, as a consequence of the accumulation of frustration events in the RTS of the random variables in the perimeter of the cluster.

It is also worthwhile to comment on the specific value of α. One can do this by defining an oversimplified RTS generalized dynamics in which Eq. (7) is replaced with

$$\mu_{k,t}=\mu_{0,t}(k+1)^{-\alpha} \tag{16}$$

and $\mu_{0,t}$ is defined through the normalization condition. It is not difficult to realize that for $\alpha<1$, the process results in a compact cluster. Indeed, the probability that a bond does not grow after k events, $\Pi_{j=1}^{k+1}(1-\mu_0 j^{-\alpha})$, goes to zero as $k\to\infty$, which means that all bonds will, sooner or later, grow.

The memory screening is effective and generates a fractal cluster only for $\alpha>1$. For $1<\alpha<2$ the screening is ''weak'' whereas for $\alpha>2$ it is ''strong.'' The difference can be appreciated by observing that for $\alpha>2$ there is a finite probability that an infinite avalanche occurs. We skip the derivation of this result, which totally parallels the arguments used for a closely related model [22], and stress that, if an infinite avalanche starts at time t_0 on the bond i_0, none of the bonds which are in $\partial\mathcal{C}_{t_0}\backslash\{i_0\}$ ($\backslash$ means except) will ever grow in the future. This means that they can be considered as frozen. For $1<\alpha<2$ infinite avalanches occur with zero probability, the screening effect is weak because one can never exclude the possibility that a bond which has waited for an arbitrarily long time k on the perimeter set will be selected at some future time. This will reflect in the peculiar implementation that the freezing condition [7] will have in the application of the FTS to IP and related models.

Finally we note that this feature of the dynamics allows us also to appreciate the difference in the fractal dimension of IP with trapping in versions I and II. This difference is somewhat at odds with the general expectation that ''universal'' properties, such as D_f, should not depend on the microscopic details of the dynamics. A trapped region in the first version of IP with trapping would not be trapped, because of only one bond. To understand how this difference is ''scale invariant'' one can imagine a process that, starting from a point A at $t=0$, encloses a region of size R and reaches at time t the site B, neighbor of A. This region would be trapped in the first version, but still open in the second. The probability that trapping will occur also in the second version is the probability that the bond A—B grows. This will, however, be of order $t^{-\alpha}$ because the age of the bond A—B is of order t. The ratio of the probabilities of trapping of a region of size R in the two versions will also depend on R through a power law. This represents a real ''scale-invariant'' difference between the two processes which is expected to affect also the value of the fractal dimension.

B. The scale-invariant ''global'' dynamics for IP

It has been shown [20] that if a growth process has a scale-invariant growth rule and an attractive fixed point in a

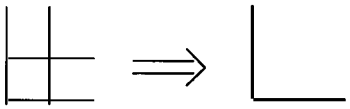

FIG. 5. Coarse graining of the lattice geometry. The eight-bond configuration at left is rescaled into the two-bond configuration at right.

given space of dynamical rules, this scale-invariant growth rule will be of bond type even if the rule at the microscopic scale is of a different nature (e.g., a site rule, or a rule with diagonal bonds). Here we will address, starting from the above considerations, the problem of the individuation of the scale-invariant dynamics for IP.

Let us start from a microscopic bond rule. We consider how the dynamics changes under a scale transformation. First of all we define a coarse-graining procedure, shown in Fig. 5: the eight bonds in the left part of the figure are mapped into the two coarse-grained bonds at the right. We consider the renormalized dynamics described in terms of effective quenched variables that refer to the coarse-grained bonds. We call the random variables for the bonds at the starting scale ϵ_i, $i=1,\ldots,8$ and the effective variables of the rescaled bonds $\epsilon_j^{(1)}$, $j=1,2$. The $\epsilon_j^{(1)}$ are functions of the ϵ_i,

$$\epsilon_j^{(1)}=F_j(\epsilon_i, i=1,\ldots,8) \quad \text{with} \quad j=1,2, \tag{17}$$

which would be the outcome of a real space renormalization group (RSRG) treatment of the dynamics of IP without proliferation. It is enough in this case to identify the scale-invariant dynamics from general considerations, similar to those used in Ref. [10].

In passing from one scale to the other, we require that the coarse-grained variables and their dynamics keep the relevant aspects of the process at the smaller scale. In this way the scale transformation eliminates only the irrelevant aspects of the dynamics.

In the particular case of IP, the dynamics is determined by the extremal statistics: the bond with the smallest variable grows. It is natural to require that this extremal property of the dynamics will be retained at all scales. In other words, we shall determine the $F_j(\ )$ in such a way that the dynamics at the smallest scale can be described, at the larger scale, by the growth of the coarse-grained bond with the smallest variable $\epsilon_j^{(1)}$. In Fig. 6 we show a coarse-graining procedure for extremal dynamics [10]. In the left side of the figure there are two paths leading to cell B (respectively, to points x_1, x_2), composed by a set of quenched variables $\{\epsilon_i\}_b$ ($\{\epsilon_i\}_{b'}$). Each path is characterized by the largest variable in the set (saddle point). The path with the smallest saddle point is the best one and will compete with the best path leading to cell A. At this point, we identify the block variable ϵ_A (ϵ_B) with the saddle point of the best path leading to the corresponding cell:

$$\epsilon_A=F_A[\{\epsilon_i\}_a]=\min_a[\max_i\{\epsilon_i\}_a]. \tag{18}$$

This should be compared with the corresponding block variable ϵ_B for B. Of course the distribution of ϵ_A and ϵ_B will now become rather complex. However, it will be the same for all the coarse-grained bonds. We have seen before that

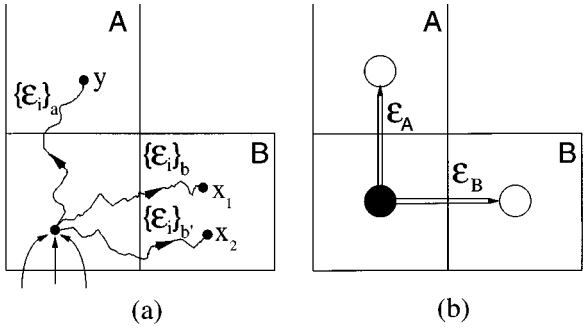

FIG. 6. Renormalization scheme for the extremal dynamics: (a) dynamics at the smaller scale; (b) the rescaled dynamics. The two paths leading to cell B (respectively, to points x_1, x_2) are composed by a set of quenched variables $\{\epsilon_i\}_b$ ($\{\epsilon_i\}_{b'}$). Each path is characterized by the largest variable in the set (saddle point). The path with the smallest saddle point is the best one and will compete with the best path leading to cell A.

the competition between quenched variables is actually independent of the initial distribution. This means that, at any scale, we can always consider for this distribution the flat one. So, we conclude that the coarse-grained dynamics is *intrinsically* scale invariant.

The only assumption made in our RG scheme is that of neglecting certain correlations between block variables. A full RSRG treatment of the dynamics of IP would allow us to go beyond this approximation and to assess whether the eventual correlations vanish in the asymptotic scale-invariant dynamics [13].

C. Fixed scale transformation for IP: The ''scale-invariant local dynamics''

We have seen that IP can be described in a way similar to a stochastic growth with annealed disorder. Once we have mapped IP onto a stochastic dynamics using the quenched-stochastic transformation we can compute its fractal dimension D_f using the fixed scale transformation approach. This method is based on the possibility of dealing separately with the two limits in which the fractal properties of such a structure are well defined: $r\to\infty$ and $t\to\infty$ [7]. The former is introduced using a scale-invariant growth rule, the latter usually (as for DBM) is introduced considering the growth in a frozen region of the structure.

While RG approaches are based on the scale invariance of the process under rescaling of the relevant parameters, FST is based on the invariance of the statistical properties of the fractal structure under translation, at a fixed scale, in the growth direction of the process. The FST approach is developed in two steps.

(1) One takes an intersection of the structure with a line orthogonal to the growth direction. This intersection is treated as a random Cantor set with fractal dimension $D_f'=D_f-1$, because of the theorem of the additivity of the codimension [23]. The generators of the Cantor set (see Fig. 13) have weights C_1 and C_2, with $C_1+C_2=1$. They are the basic configurations for the intersection set and define its statistical properties. In fact, the fractal dimension D_f' can be written as [24] $D_f'=\ln(C_1+2C_2)/\ln 2$.

(2) One computes the conditional probabilities to have a configuration of type i on a given intersection set followed at

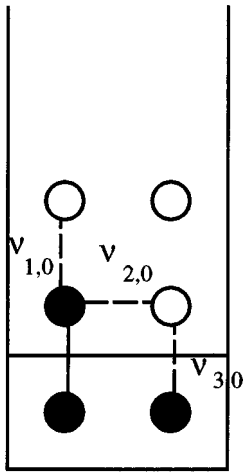

FIG. 7. An example of initial configuration in the growth column for the FST scheme of calculation.

the next intersection set by a configuration of type j $(i,j=1,2)$. These conditional probabilities $M_{i,j}$ form a 2×2 matrix, called FST transfer matrix M. The relation between the weights C_1, C_2 of the basic configurations, on which the FST matrix acts, at the intersection k, and those at the intersection $k+1$, is given by

$$\{C_i^{(k+1)}\}=M\{C_i^{(k)}\}. \tag{19}$$

The fixed point solution of (19) is

$$C_1^*=\left(1+\frac{M_{1,2}}{M_{2,1}}\right)^{-1}. \tag{20}$$

Equation (20) gives the asymptotic statistical properties of the intersection set. In fact, the $M_{i,j}$ can be expressed as lattice path integrals over all the growth histories of the process leading to a configuration i followed in the growth direction by a configuration j. FST performs the calculation of the $M_{i,j}$ with the simplifying assumption that growth occurs only in a ''growth column'' of indefinite height, with a two-site basis, and with a ''frozen'' starting configuration i (Fig. 7). The scheme of calculation can be refined with the introduction of fluctuating boundary conditions and of the empty configurations [25] that extend the growth process outside the growth column. The FST has been applied to a variety of models, giving very good estimations of their fractal dimension [7]. However, in order to obtain scale-invariant results one has to use the scale-invariant dynamics of the process in the calculation of the $M_{i,j}$ [20,21].

Now we try to define a FST approach for IP based on the use of RTS. In the peceding subsection we have seen how to deal with the limit $r\to\infty$, i.e., how bonds can represent ''coarse-grained'' lattice elements, using the ''scale-invariant growth rule.'' Since the nature of ''freezing phenomena'' in IP is quite different from that of DBM, we have to introduce the limit $t\to\infty$ in a peculiar way defining a ''local dynamics.'' While in DBM the nature of freezing is referred to regions of the lattice, in IP it is referred only to single bonds. In fact in DBM freezing is an electrostatic phenomenon, so if a point has a very low value of the electrostatic field it is reasonable to think that it exists in an extended region surrounding that point with low values of the field, too. This characteristic allows us to consider only the bonds in the growth column to deduce the fractal properties of the structure. In fact, this column is thought to be on the surface of such a region of the structure. In IP, freezing is a probabilistic phenomenon, referred only to single bonds. So, it is possible to have a frozen bond on the perimeter (a bond with a great frustration index θ) near to an active bond (small θ). This is also the reason the perimeter has the same fractal dimension of the structure itself.

How can we deduce the fractal properties of the structure generated by IP, in the limit $t\to\infty$, considering explicitly only the bonds inside the growth column? To answer this question we need to find the scale-invariant ''local'' dynamics. The scale-invariant growth rule we have found for IP is the rule of the ''global'' dynamics. Using this rule together with the RTS approach, we can evaluate the statistical weight of any path generated by the IP process, at a generic scale. However, in order to use the global growth rule it is necessary to know the whole history of the process from the initial instant $t=0$. In fact, the probability of one growth step of the path depends on the RTS of every bond in the perimeter of the structure, and the form of the RTS is determined by the past growth history.

On the other hand, the FST approach is based on the evaluation of the statistical weight of paths inside the growth column, considering explicitly only the bonds inside this column and the others in the perimeter just in a mean way. So, to apply the FST approach to IP, we have to modify the RTS equations in such a way as to be able to evaluate the ''transition probabilities'' $M_{i,j}$ related to the FST method, considering *explicitly* only the bonds inside or near the column and *implicitly* the others. In doing so we shall recognize the *scale-invariant local dynamics* through the definition of *scale-invariant asymptotic avalanches*.

We consider a growth column on the perimeter of the already infinite structure $(t\to\infty)$. We are going to show that the RTS dynamics which corresponds to the *local* scale-invariant dynamics, as in Ref. [10], is obtained by (i) considering only bonds inside the growth column; (ii) imposing that any ''active'' bond i in the column can grow only if the value of its variable ϵ_i is less than $p_c=1/2$; the idea is that if $\epsilon_i>p_c$ for all the bonds in the growth column, growth will occur at some other place in the structure outside the growth column; and (iii) requiring that the largest of the variables which participate in the growth process, which is the variable on the initial bond, has exactly $\epsilon_i=p_c$. This local dynamics derives directly from the global dynamics. To see this it is sufficient to observe that in Eq. (7) we can separate, in the product inside the integral, the contribution from the part of the interface $\partial\mathcal{C}_t^{\rm in}$ inside the column, and that over the bonds $k\in\partial\mathcal{C}_t^{\rm out}$ outside the column:

$$\nu_{i,t}=\int_0^1 \frac{\rho_{i,t}(x)dx}{\int_x^1 \rho_{i,t}(z)dz} Z_t^{\rm in}(x) Z_t^{\rm out}(x), \tag{21}$$

where

$$Z_t^{\rm out}(x)=\prod_{j\in\partial\mathcal{C}_t^{\rm out}} \int_x^1 \rho_{j,t}(y)dy \tag{22}$$

and $Z_t^{\rm in}(x)$ is analogously defined. Now, if the bond $i \in \partial\mathcal{C}_t^{\rm in}$ actually grows and its value is $\epsilon_i = p_c$, we can interpret $Z_{t+1}^{\rm out}(x)$ as the probability that the minimum variable outside the column is larger than x. It follows straightforwardly that $Z_{t+1}^{\rm out}(x)=1$ for $x<p_c$. Indeed the minimum variable in $\partial\mathcal{C}_t^{\rm out}$ will surely (i.e., with probability 1) be larger than $\epsilon_i = p_c$ in view of our assumption for the event at time t. On the other hand, if the cluster is very large ($t\to\infty$), we can appeal to the properties of the histogram distribution [8], and conclude that there will be variables in $\partial\mathcal{C}_t^{\rm out}$ whose value will be arbitrarily close to p_c. In fact, the histogram distribution for the perimeter variables of an asymptotically large structure is a step function. This can be proven rigorously as a property of the asymptotic structure [18]. The RTS method [8] allows us to follow the evolution of the histogram and to show that the step function corresponds to the attractor for the dynamics of the system. Therefore, in the limit $t\to\infty$, we can conclude that $Z_{t+1}^{\rm out}(x)=0$ for $x>p_c$. In summary $Z_{t+1}^{\rm out}(x)$, as $t\to\infty$, tends to a step function at p_c. When inserted in Eq. (21) the integration variable x runs *only up to* p_c, and the contribution from the bonds outside the column disappears. Therefore, going back to the RTS variable k, Eqs. (7)–(9) for the local dynamics read

$$\mu_{k,t} = \int_0^{p_c} dx\; p_{k,t}(x) \prod_\theta \left[1 - P_{\theta,t}(x)\right]^{n_{\theta,t} - \delta_{\theta,k}}, \quad (23)$$

$$m_{k,t}(x) = \begin{cases} \dfrac{p_{k,t}(x) \displaystyle\prod_\theta \left[1 - P_{\theta,t}(x)\right]^{n_{\theta,t} - \delta_{\theta,k}}}{\mu_{k,t}} & \text{for } x < p_c \\ 0 \text{ for } x > p_c, \end{cases} \quad (24)$$

and

$$p_{\theta+1,t+1}(x) = \begin{cases} p_{\theta,t}(x) \displaystyle\int_0^x dy \frac{m_{k,t}(y)}{1 - P_{\theta,t}(y)} & \text{for } x \leqslant p_c \\ p_{\theta,t}(p_c) \displaystyle\int_0^{p_c} dy \frac{m_{k,t}(y)}{1 - P_{\theta,t}(y)} & \text{for } x \geqslant p_c, \end{cases} \quad (25)$$

where $n_{\theta,t}$ is now the number of the bonds, inside the column, which have age θ.

We need still to motivate the choice of $\epsilon_i = p_c$ for the initiator of the local process. Note that, up to now, we have only imposed on the local dynamics the $t\to\infty$ condition, which implies that the local event is occurring in the presence of an ''infinite'' cluster. The requirement that $\epsilon_i = p_c$ results from imposing scale invariance on the local dynamics, i.e., from the limit $r\to\infty$ [7].

In order to see this, let us recall the definition of avalanches in IP: an avalanche is defined as a temporally consecutive set of growth events causally and spatially connected to a first growth event. The bond related to this first growth event is called the *initiator* of the avalanche. To make this definition clear we focus our attention on an active bond l on the perimeter of the structure which grows at the instant t_0; the avalanche with initiator l is defined as the *temporal sequence* of growth events which begins at t_0 and ends when a bond that was on the perimeter *before* t_0 will grow.

From this definition one deduces that every growing bond can be considered the initiator of an avalanche. In particular, the whole structure can be seen as the avalanche related to the first grown bond at $t=0$. This means that any avalanche is made by other subavalanches in a hierarchical order. The number of subavalanches in which we can decompose an avalanche is obviously equal to its size s.

Let us analyze the properties of an avalanche taking place on the perimeter of the infinite structure ($t\to\infty$). In this limit, if the initiator has a variable $\epsilon_i = p$, we can extract the statistics of this avalanche process from Eqs. (23)–(25) where p_c is replaced by p. It is obvious from these equations that the size of the avalanche and its statistical properties depends only on the value $\epsilon_i = p$ of the variable of the initiator i. It is known [12] that the distribution of the size of avalanche has scale-invariant properties only if $p \equiv p_c$. Avalanches with $p > p_c$, in view of the acceptance profile, can be neglected as really rare events (indeed these would have an infinite duration, and on the grounds of our previous discussion can be neglected). On the contrary, avalanches starting with $p < p_c$ will have a finite lifetime $s_0 \sim |p - p_c|^{-1/\sigma}$. These cannot be thought of as scale-invariant events. Only for $p = p_c$ will the process defined by Eqs. (23)–(25) be scale invariant. If the initiator has $\epsilon_i = p_c$, the process will sample its duration out of a scale invariant distribution, and therefore it will be, itself, scale invariant. This justifies the use of Eqs. (23)–(25) in the application of the FST to IP. This local dynamics has the following properties.

(a) The dynamics is defined only in terms of the local variables inside the growth column. The presence of the infinite perimeter enters only via the variable $\epsilon_i = p_c$ of the initiator. In this way we do not need to know the RTS of the other perimeter bonds.

(b) The growth probabilities ν_{i,t_0+s}, calculated at each time step t_0+s, are not normalized to 1, that is to say, $\Sigma_{i \in \partial\mathcal{C}_{t_0+s}^{\rm in}} \nu_{i,t_0+s} < 1$. This implies the existence of a probability

$$W_{t_0+s}(\varepsilon_i) = \prod_{j \in \partial\mathcal{C}_{t_0+s}^{\rm in}} \int_{\varepsilon_i}^1 dx \rho_{j,t_0+s}(x) \geqslant 0 \quad (26)$$

that the process stops. In this case the activity moves to another region of the perimeter. This is a relevant feature of the local avalanche dynamics, and it reflects the dynamical evolution of IP.

In the FST calculation scheme for problems such as DBM the growth probability distribution is usually normalized in the growth column in order to allow the growth interface to reach regions far from the starting one. This allows us to reach more easily the geometrical ''freezing'' limit $t\to\infty$ in the growth column. This is an important assumption, because in models like DBM, the fractal properties of the frozen regions are different from these of the growing perimeter.

In IP these problems do not exist, because *when an avalanche with initiator at p_c stops it leaves a local structure with the same statistical properties of the bulk of the whole cluster*. In fact, after an avalanche has stopped, all the local

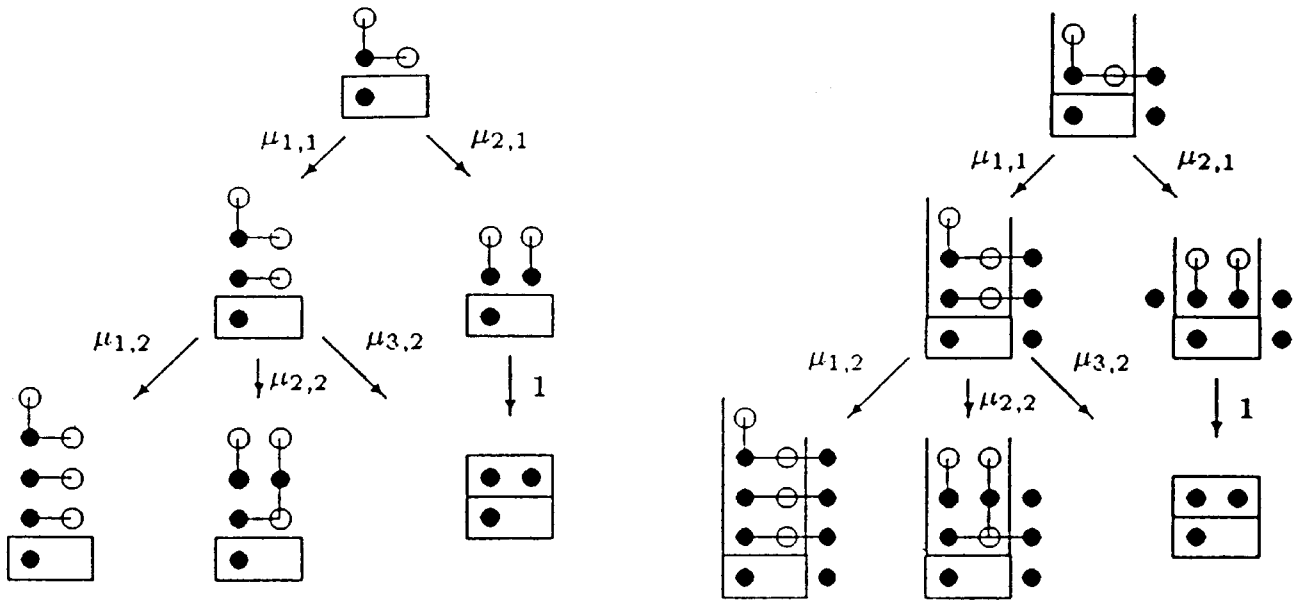

FIG. 8. (a) Graphical scheme for the calculation of $M_{1,2}^{\mathrm{op}}$ (at the second order); (b) graphical expansion for the calculation of $M_{1,2}^{\mathrm{cl}}$ (second order). The black dots are the occupied sites and the labels i,j of the $\mu_{i,j}$ (the $\mu_{i,j}$ are the growth probability of the stochastic process) indicate, respectively, the active bond (from left to right and from top to bottom) and the order of the process.

perimeter bonds will have potentials greater than p_c, and we know from the acceptance profile that bonds with such values of the potential will not grow.

Therefore the lack of normalization of the GPD for the local dynamics is totally consistent with the FST scheme. This is an interesting and relevant aspect of the local scale-invariant dynamics for IP. In fact, we have verified that if one substitutes p_c with 1 in Eqs. (23)–(25), using the global scale-invariant dynamics instead of the local one, one forces the process to occupy all the bonds in the column. This produces a compact structure with $D_f=2$. In this respect it may be useful to comment about how the present approach compares with the preliminary one developed in 1990 by Pietronero and Schneider [9]. In that paper the basic idea of the quenched-stochastic transformation is introduced. However, its implementation in the FST scheme was highly simplified and heuristic. In some sense the FST matrix elements are computed from a sort of exact enumeration of the first few steps and, for example, the questions of the self-organization and the scale-invariant dynamics could not be addressed. The approach discussed here represents instead a rather complete and systematic theoretical method for these extremal problems.

D. Calculation of the fractal dimension of IP

Now we proceed to the calculation of the fractal dimension of IP in the FST scheme. This scheme is based (see [6,7]) on two main approximations.

(1) Only periodic boundary conditions with variable period λ are allowed for the growth column.

(2) In practice we consider only two values of the period λ: $\lambda=0$ (closed boundary conditions) and $\lambda=\infty$ (open boundary conditions). To each case we assign a weight in a self-consistent way, as discussed in [7].

Note that for IP and for percolation problems in general this ''open-closed'' approximation is particularly accurate.

The calculation of the FST matrix elements $M_{i,j}^{\mathrm{op}}$ and $M_{i,j}^{\mathrm{cl}}$ for open and closed boundary conditions, respectively, is performed by using the graphical expansion shown in Fig. 8 (for more details see [6,7]), where the $\mu_{k,t}$ are given by Eq. (23). We call order n of the process the number of bonds grown starting from the initial configuration (see Fig. 7). The bond connecting the frozen cell to the occupied site is the initiator of the avalanche with variable p_c. Let us call $M_{i,j}^{\mathrm{op}}(n)$ and $M_{i,j}^{\mathrm{cl}}(n)$ the matrix elements at order n for open and closed boundary conditions, respectively. Usually, for both boundary conditions, at a given order n, one directly evaluates the $M_{i,2}(n)$, getting the $M_{i,1}(n)$ elements from the normalization condition $\Sigma_j M_{i,j}(n)=1$.

For example, let us evaluate $M_{1,2}^{\mathrm{op}}(n=2)$. At the first step we have two ''active'' bonds in the column (see Fig. 8) that we indicate as 1,1 and 2,1, where the first number is the bond label and the second number is the order n. Everyone has $\rho_{i,1}(x)=p_{0,0}(x)=1$ with $i=1,2$. From Eq. (23) with $p_c=\frac{1}{2}$ one gets

$$\mu_{i,1}=\int_0^{1/2} dx(1-x)=\tfrac{3}{8}\,. \tag{27}$$

For $i=2$ we have the first path contributing to $M_{1,2}^{\mathrm{op}}$

$$M_{1,2}^{\mathrm{op}}(n=1)=\tfrac{3}{8}\,. \tag{28}$$

We can also calculate the probability P_1 that the avalanche ends already at the first order. From Eq. (26) with $\varepsilon_i\equiv p_c=1/2$ we have

$$P_1=\left(\int_{1/2}^{1} dx\right)^2=\tfrac{1}{4}\,. \tag{29}$$

To compute the second order contribution to $M_{1,2}^{\mathrm{op}}$ we let the bond 1,1 grow at time $t=1$. Two new bonds enter the pe-

rimeter with uniform density (Fig. 5). The density of the bond 1,1 becomes, after it grows,

$$m_{1,1}(x)=\tfrac{8}{3}(1-x)\,\theta(\tfrac{1}{2}-x). \tag{30}$$

At order 2 the bond 2,1 is labeled 3,2, and has updated density

$$\rho_{3,2}(x)=\tfrac{8}{3}\min(x,\tfrac{1}{2}). \tag{31}$$

Now we can compute $\mu_{3,2}$, which is the only second order contribution to $M_{1,2}^{\rm op}$ applying Eq. (23) again:

$$\mu_{3,2}=\tfrac{11}{72}. \tag{32}$$

So, at the second order we obtain

$$M_{1,2}^{\rm op}(n=2)=\mu_{2,1}+\mu_{1,1}\mu_{3,2}=\tfrac{3}{8}+\tfrac{3}{8}\ \tfrac{11}{72}. \tag{33}$$

Such calculations can be pursued to any higher order, considering at any order all the paths contributing to $M_{1,2}^{\rm op}$ In the same way we calculate $M_{2,2}^{\rm op}$

Then we calculate, using the same method, the matrix elements for closed boundary conditions $M_{i,2}^{\rm cl}$ For a given order n it is possible to express the weights $C_1(n)$ and $C_2(n)$ of the two-cell configurations in the intersection set in terms of the $M_{i,j}^{\rm op}(n)$ and $M_{i,j}^{\rm cl}(n)$ using the formula (see [6,7])

$$C_1(n)=\frac{M_{1,2}^{\rm cl}+M_{2,1}^{\rm cl}-\frac{3}{2}M_{2,1}^{\rm op}-[(\frac{3}{2}M_{2,1}^{\rm op}-M_{1,2}^{\rm cl}-2M_{2,1}^{\rm cl})^2-4M_{2,1}^{\rm cl}A]^{1/2}}{2A},$$
$$C_2(n)=1-C_1(n),$$
$$A=M_{1,2}^{\rm cl}+M_{2,1}^{\rm cl}-\tfrac{3}{2}(M_{1,2}^{\rm op}+M_{2,1}^{\rm op}), \tag{34}$$

where we omitted for simplicity the n dependence of the matrix elements.

The fractal dimension at the order n is given by

$$D_f(n)=1+\frac{\ln[1+C_2(n)]}{\ln 2}. \tag{35}$$

Unfortunately, while for DBM we have an exponential convergence [6,7] with respect to the order n of the matrix elements, for IP the convergence is power-law-like. This should be expected, in view of the power law behavior of $\mu_{k,t}\sim(k+1)^{-\alpha}$ (memory effect) discussed previously. It is therefore necessary to extrapolate the results to $n=\infty$. In order to perform the calculations needed in practice we have developed a computer algorithm which executes the calculation of the growth probabilities, the updating of the RTS, and stores all the growth histories. The integrals are performed with the method of Gaussian integration over 100 points in $[0,1/2]$, because the RTS, in the *scale-invariant local dynamics*, is constant in $[1/2,1]$.

In Table I we report the RTS-FST values of the IP fractal dimension for the various orders, compared with known analytical and simulation results. Our result is in very good agreement both with numerical simulations and with known analytical values. The same scheme can be easily applied to the case of IP with trapping for both site and bond trapping. Before treating these two cases, we want to address briefly the problem of the scale-invariant dynamics. If we assume the coarse-grained random variables on the lattice to be statistically independent, the scale-invariant local dynamics is completely specified by the value of p_c, like for IP without trapping. The scale-invariant dynamics for IP with trapping is the same as for IP. This can be verified, for example, in [1], where one sees that the acceptance profile of IP with trapping tends asymptotically, although with lower speed and asymmetrically, to the same step function found for IP. Another way to verify our argument is the following: if we consider a trapped region of the lattice, the growth events on the perimeter are statistically independent from the bonds

FIG. 9. Left side of the figure: an example of the introduction of trapping I in the FST scheme. Right side of the figure: an analogous example for the implementation of trapping II. One can see in both cases how the path generating trapping contributes to $M_{i,1}^{\rm cl}$

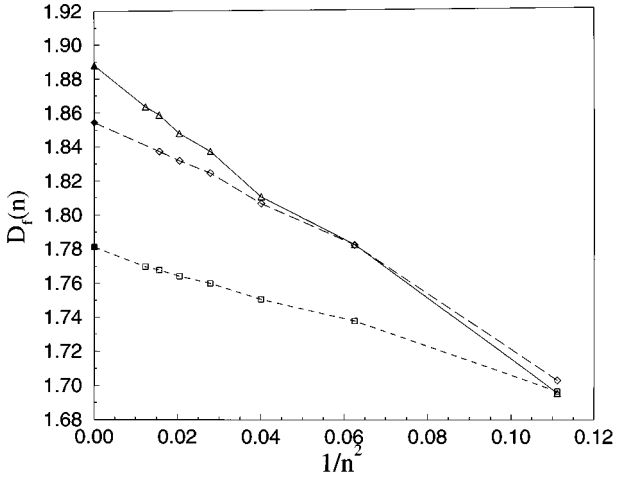

FIG. 10. Values of the fractal dimension $D_f(n)$ for IP ($\triangle$), IP with site trapping ($\square$), and IP with bond trapping ($\diamond$) via FST calculations versus $1/n^2$ for $n=3,\ldots,9$. The extrapolation gives the asymptotic value $D_f(\infty)$ (filled symbols).

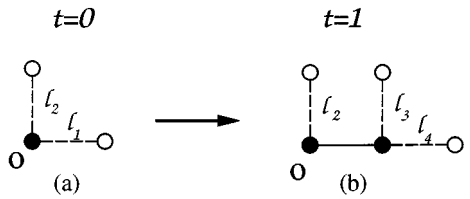

FIG. 11. Starting situation for DIP: (a) the black dot indicates $\mathcal{C}_0$ and the dotted segments indicate the active bonds; (b) the situation after the growth of the horizontal active bond.

inside the trapped zone. This means that trapping does not have, asymptotically, any influence on growth in the external perimeter. So, the scale-invariant dynamics is the same.

In the FTS scheme trapping appears only for closed boundary conditions. In fact (see Fig. 9), a region in the growth column can be trapped only if it has occupied sites or bonds from both sides and this requires at least three vertical lines of sites. In the open boundary condition case we will get the same numerical results found for IP without trapping. Now, for IP with trapping one can see (Fig. 9) that all paths generating trapping contribute directly to $M_{i,1}^{\mathrm{cl}}$.

In Table I we report the values of the fractal dimension vs n for both types of trapping, and we compare them with known simulation values. No previous analytical results are available for IP with trapping. Also in this case our analytical results fit very well with known values. In Fig. 10 we show the behavior of $D_f(n)$ versus $1/n^2$, for IP, IP with site trapping (trapping I), and IP with bond trapping (trapping II), with the extrapolation to $n=\infty$. The fact that the $D_f(n)$ fits well with a power law $1/n^2$ can be understood [8] by the large time limit of the $\mu_{k,t}$, which goes to zero with k as $1/(k+1)^2$. In fact, the ''older'' bond in the growth column has an age which coincides with the order n of FST calculations.

The main reason for the relatively poor approximation of our results for IP with site trapping (see Table I) is that, while the FST scheme is based on a bond dynamical rule, as suggested by Ref. [20], in the site trapping model, we use a site rule to identify trapped configurations. This trapping rule is not expected to be scale invariant [20], and it is therefore natural that this inadequacy influences the numerical result. Yet, the value we find might be considered as a nontrivial lower bound to D_f^I

E. The directed invasion percolation

In this part of the paper we study a directed version of IP, the directed invasion percolation. The model is the same as for IP, but with the following growth rule: at $t=0$ the active bonds are the vertical upper bond and the horizontal right bond leaving the site O [Fig. 11(a)]. At $t=1$ the active bond with the smallest variable grows [the horizontal one in Fig. 11(a)]. After the growth, we add to the perimeter the upper vertical bond and the right horizontal bond connected with the just grown bond [Fig. 11(b)]. And so on.

From the dynamics we have defined it appears clear that the DIP cluster, if one starts from site O, will develop itself entirely in a lattice quadrant with vertex in O and will have as mean growth direction the quadrant bisector. We can apply to DIP the quenched-stochastic transformation, using the RTS $p_{k,t}(x)$ and the GPD $\mu_{k,t}$ for the active bonds and the updating rule for the RTS after a growth step, in the same way as for IP. The difference with respect to IP is that DIP is an anisotropic model, because it has a mean growth direction. In the same way as IP is the dynamical, invasive, version of critical percolation, DIP can be viewed as the dynamical version of directed percolation (DP).

Let us recall briefly the main properties of DP [26]. We label the four directions on the lattice with the cardinal points: east and west are the horizontal directions and north and south the vertical ones. The positive directions are north and east. We orient the bonds, assigning to each one an arrow, in the positive direction and, as for percolation, we assign to each bond a random number. A threshold p is fixed and one introduces the probability $P(A\rightarrow B;p)$ to find a path connecting two points A and B, composed by bonds with random variables less than p and following the arrows assigned to the bonds. For percolation, if $p<p_c=1/2$ one has a correlation length $\xi\propto|p-p_c|^{-\nu}$, with critical exponent ν. For DIP we have an analogous situation with a different critical threshold $p_c^{(\mathrm{dir})}=0.644\,071>p_c$ and, because of the anisotropy of DIP, two correlation lengths: $\xi_{||}$, parallel to the growth direction, and $\xi_{\perp}$, perpendicular, with the following scaling behavior for $p<p_c^{(\mathrm{dir})}$:

$$\xi_{||}\propto(p_c^{(\mathrm{dir})}-p)^{-\nu_{||}} \quad \text{and} \quad \xi_{\perp}\propto(p_c^{(\mathrm{dir})}-p)^{-\nu_{\perp}},$$

with $\nu_{||}>\nu_{\perp}$.

The DP clusters have the following properties: (1) for $p<p_c^{(\mathrm{dir})}=0.644\,071$ there is no percolating cluster; (2) for $p>p_c^{(\mathrm{dir})}$ there is a percolating, infinite and compact, cluster with fractal dimension $D_f=2$; and (3) for $p=p_c^{(\mathrm{dir})}$ there is an infinite percolating cluster with fractal dimension $D_f=1.748\ldots$ [27]. We claim that, as for IP, the DIP model produces spontaneously an asymptotic structure with the same geometrical properties of the infinite percolating cluster of DP at the critical threshold $p_c^{(\mathrm{dir})}$.

Indeed the RTS calculations of Ref. [8] can be applied to the case of DIP as well. One can define a histogram function, which is the histogram $\Phi_t(x)$ of the values of the variables on the perimeter bonds, and write down a histogram equation like Eq. 15. The asymptotic behavior of $\Phi_t(x)$ will be

$$\lim_{t\rightarrow\infty}\Phi_t(x)=\frac{1}{1-\pi_c}\,\theta(x-\pi_c), \tag{36}$$

where the parameter π_c coincides with the DP threshold $p_c^{(\mathrm{dir})}=0.644\,071$ [27]. This supports the hypothesis that between DIP and DP there is the same link existing between IP and critical percolation.

Now we apply the FST approach to DIP to compute its fractal dimension. The scale-invariant local dynamics can be determined by the same arguments used for IP. What we find is that the local dynamics to use in the FST growth column is the same used for IP, Eqs. (23)–(25), where we have to substitute $p_c=1/2$ with $p_c^{(\mathrm{dir})}=0.644\,071$.

In applying FST to DIP one has to face a technical problem. In fact, the FST analyzes the intersection between the asymptotic structure and a line [6,7]. This intersection is a

random Cantor set (Fig. 13) in which the weights of the generators are determined from the dynamics of the model, expressed by the FST matrix $\{M_{i,j}\}$. IP is an isotropic growth model. So, the orientation of the line we intersect with the structure is not relevant. For anisotropic systems, like DBM which has a definite growth direction, the intersection is usually taken in the direction perpendicular to the direction of growth [7]. The resulting random Cantor set (fragmentation process) is therefore isotropic. In DIP, one would have to tilt the lattice by $\pi/4$ in order to perform the FST ''along'' the growth direction. This would pose problems of renormalization of a dynamics with diagonal bonds which is known to be problematic [20]. For this reason we choose to tilt the direction in which the FST evolves by $\pi/4$, with respect to the growth direction (the FST evolves in the north direction, whereas the growth direction is northeast). This choice has the price that the intersection with a horizontal line will result now in an anisotropic Cantor set. This can be described by three generators C_2, C_1, and C_0 (Fig. 13) satisfying the condition $C_0+C_1+C_2=1$.

So, we have three fundamental configurations on the intersection set and the FST matrix $\{M_{i,j}\}$ will be a 3×3 one:

$$\begin{pmatrix} M_{0,0} & 0 & M_{2,0} \\ 0 & M_{1,1} & M_{2,1} \\ M_{0,2} & M_{1,2} & M_{2,2}, \end{pmatrix}, \tag{37}$$

where $M_{1,0}=M_{0,1}=0$ in that there cannot be a transition between the 0 and 1 configurations, and with the following normalization condition for the probabilities: $\Sigma_{j=1}^{3} M_{i,j}=1$ for $i=1,2,3$. In open boundary conditions one has $M_{0,0}^{\mathrm{op}}=1$.

The fractal dimension is again given by

$$D_f'=\frac{\ln(1+C_2)}{\ln 2}, \tag{38}$$

where C_2 is the fixed point solution of Eq. (37).

The probabilities for open and closed boundary conditions in the open-closed approximation have to be obtained from the void distribution $P^{(\mathrm{anis})}(\lambda)$ of an anisotropic random Cantor set, while for IP we used the usual void distribution of an isotropic Cantor set [29]. In Appendix B we compute the $P^{(\mathrm{anis})}(\lambda)$ and report also the equation for the weights C_i from which one gets the fixed point values. The results are shown in Table I, and compared with known results. Note that in passing from the dimension of the intersection set to that of the cluster, one generally assumes that the fractal is isotropic. This point might be nontrivial in DP. It is, however, clear that in any case our result refers to an intersection of the cluster with a line at an angle of $\pi/4$ with the growth direction. Within this assumption of isotropy, this value results in excellent agreement with that found for DP ($D_f^{\mathrm{DP}}=1.748\ldots$ [27]). This result, together with the asymptotic behavior of the DIP histogram $\Phi_t(x)$, supports the hypothesis that DIP is the self-organized dynamical version of critical DP.

III. ANALYSIS OF THE CRITICAL AVALANCHES FOR IP

In this section we will address the problem of the analysis of the distribution of critical avalanches in invasion percolation. We have seen in the preceding section that avalanches have a hierarchical structure and that in the limit $t\to\infty$ their duration (or size) depends only on the value of the random variable of the initiator.

Until now the analysis of the size distribution of avalanches has been based mainly on the combination of computer simulation of the process and scaling ansatz obtained in analogy with the distribution of clusters in usual percolation [11,12]. Based on this analogy, the following functional form for the size distribution is assumed:

$$D(s;p)=s^{-\tau}f(|p-p_c|s^{\sigma}), \tag{39}$$

where $p=\varepsilon_i$ and $p_c=1/2$ is the critical threshold for 2D bond percolation on a square lattice. The function $f(x)$ has the following properties: $\lim_{x\to 0}f(x)=\alpha\neq 0$ and for large values of x $f(x)\sim e^{-x}$. In [11,12], by an analysis of the temporal signal $\varepsilon(t)$ (the value of the smallest variable at time t) together with scaling relations the following values of τ have been obtained, respectively, by numerical simulations: $\tau\simeq 1.50$ and $\tau\simeq 1.60$. This last value seems to be the most recent and accurate.

The size s of the avalanche also includes the initiator. Thus the normalization condition for Eq. (39) will be

$$\sum_{s=1}^{\infty} D(s;p)=1 \ \forall p\in[0,1]. \tag{40}$$

We now propose a theoretical scheme for the analytical calculation of the avalanche exponent τ, based on the RTS and the FST ideas.

Usually Eq. (39) holds true for $s\gg 1$. However, if we consider the dynamics at a certain scale ℓ, we can use Eq. (39) to describe the statistics of avalanches at that scale. In this case, the normalized form of Eq. (39), for $p=p_c$ is

$$D(s;p_c)=\frac{s^{-\tau}}{\sum_{s=1}^{\infty} s^{-\tau}}. \tag{41}$$

Note that the denominator is the function Riemann zeta, $\zeta(\tau)$. From Eq. (41), valid if the initiator is at p_c, one has

$$D(s=1;p_c)=\frac{1}{\sum_{s=1}^{\infty} s^{-\tau}}=\frac{1}{\zeta(\tau)}. \tag{42}$$

We will obtain a value of τ by (a) evaluating the left-hand side using the scale-invariant local dynamics of IP and by taking into account the boundary conditions near the avalanche, and (b) inverting Eq. (42).

Let us evaluate $D(s=1;p_c)$. The event $s=1$ means that after the growth of the initiator with variable p_c the avalanche stops. Thus we consider the initiator i as grown at time t_0 and calculate the probability that the avalanche stops at time t_0+1. This will happen if all the descendant bonds of

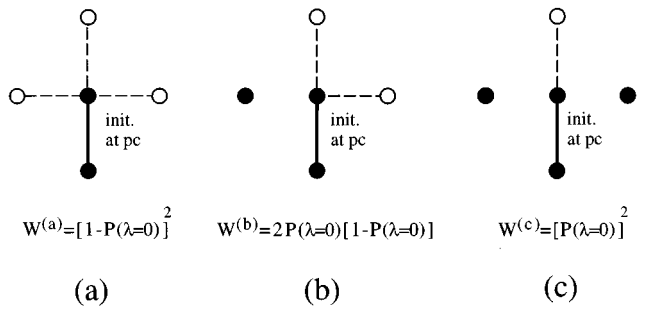

FIG. 12. Boundary conditions for the initiator of an avalanche when the initiator bond grows. ● indicates the cluster sites and ○ the perimeter ones: the filled segments represent grown bonds and the dotted ones the descendant of the initiator. One has three possibilities: (a) there is no occupied site near to the initiator′s one (three descendant bonds); (b) there is one occupied site near the initiator (two descendants); (c) both sites near the initiator are occupied (one descendant).

the initiator have variables larger than p_c. In fact, if at least one descendant of i had variable lower than p_c, the avalanche would continue because this variable would be the minimum one on the whole perimeter. In order to evaluate this probability accurately we need to take into account the environment of the initiator. In Fig. 12 we schematize all the possible boundary conditions for the initiator bond. We consider only the nearest neighbor of the initiator because we know that asymptotically the avalanches on the perimeter are influenced only by the environment near the zone where the avalanche evolves, that is to say, by other branches of the aggregate which have some perimeter bonds involved in the avalanche.

For all three cases we can evaluate the probability that the avalanche stops immediately after the initiator′s growth, conditioned by the assigned boundary conditions. The exact value of this probability, by the rule of composed probabilities, is given by the mean of the three cases. In order to compute the statistical weights of configurations (a)–(c) of Fig. 12 we use the void distribution $P(\lambda)$ of the random (isotropic) Cantor set whose generators have probabilities C_i, $i=1,2$ given by the FST calculations performed in the preceding section. We are allowed to use $P(\lambda)$ with the weights obtained by FST because for IP the perimeter has the same statistical properties as the bulk of the structure.

We remember the expression of $P(\lambda=0)$ [7] in terms of C_2:

$$P(\lambda=0)=\frac{C_2}{C_2+\frac{1}{4}(1-C_2)(3+C_2)}. \tag{43}$$

The weights of configurations (a), (b), and (c) are

$$W^{(a)}=P(\lambda\geqslant 1)/P(\lambda\geqslant 1)\equiv[1-P(\lambda=0)]^2,$$

$$W^{(b)}=2P(\lambda=0)/[1-P(\lambda=0)],$$

$$W^{(c)}=[P(\lambda=0)]^2. \tag{44}$$

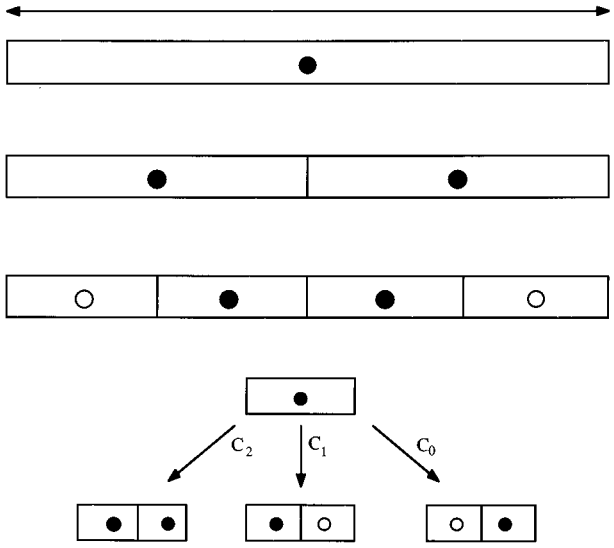

FIG. 13. Fragmentation procedure for the anisotropic random Cantor set. One starts from the system at the biggest scale, appearing as an occupied unitary cell of length L (we set $L=1$) and one proceeds by successive fragmentations governed by the weights C_i of the three generators. For the isotropic case the only difference is that we have only two generators, in that one has $C_0=C_1$.

The fixed point value of C_2 obtained from FST calculation for IP in the preceding section is $C_2\simeq 0.861$. If we introduce this value in Eqs. (43) and (44) we get $P(\lambda=0)\simeq 0.865$, and

$$W^{(a)}\simeq 0.018,$$
$$W^{(b)}\simeq 0.233,$$
$$W^{(c)}\simeq 0.749. \tag{45}$$

Now we compute the probabilities $P^{(k)}(s=1;p_c)$, $k=a,b,c$ that the avalanche stops immediately after the growth of the initiator, for the three different boundary conditions, using the RTS method. The descendants of the initiator have RTS $p_{0,0}(x)=1$, because they have just entered in the perimeter. So, one has

$$P^{(a)}(s=1;p_c)=\left(\int_{p_c}^{1}dx\ p_{0,0}(x)\right)^3=\tfrac{1}{8},$$

$$P^{(b)}(s=1;p_c)=\left(\int_{p_c}^{1}dx\ p_{0,0}(x)\right)^2=\tfrac{1}{4},$$

$$P^{(c)}(s=1;p_c)=\int_{p_c}^{1}dx\ p_{0,0}(x)=\tfrac{1}{2}. \tag{46}$$

From Eqs. (46) one obtains

$$D(s=1;p_c)=\prod_{k=a,b,c}W^{(k)}P^{(k)}(s=1;p_c)\simeq 0.435. \tag{47}$$

At this point, in order to find τ we should solve the equation

$$0.435=\frac{1}{\sum_{s=1}^{\infty}s^{-\tau}}=\frac{1}{\zeta(\tau)}. \tag{48}$$

The numerical solution of Eq. (48) gives

$$\tau = 1.5832\ldots.$$

This analytical result is in good agreement with recent numerical simulations [12], which give $\tau = 1.60$.

In order to test independently the validity of our method, we have performed numerical simulations of IP to get an estimation of τ. From the RTS scheme and the discussion of the scale-invariant local dynamics and critical avalanches, we observe that the counter $\theta(t_0+s)$ (the age) of the bonds growing during the avalanche must satisfy the following condition:

$$\theta(t_0+s) < s, \tag{49}$$

where t_0 is the time at which the avalanche starts [23].

So, if we are in the asymptotic limit (very large time), we can analyze the signal $\theta(t)$, instead of $\epsilon(t)$, in order to reconstruct the avalanche size distribution and to obtain numerical estimation of the exponent τ. This is an alternative method that allows us to count only the critical avalanches, avoiding problems of numerical approximations that one faces when one analyzes the signal $\epsilon(t)$. In fact, $\epsilon(t)$ is a real random variable, while $\theta(t)$ is an integer one. We get $\tau \simeq 1.60 \pm 0.03$, in very good agreement with our theoretical result. From the knowledge of the exponents D_f and τ one can recover, using the scaling relations reported in [12], all the other critical exponents of IP.

CONCLUSIONS

In this paper we have exploited a theoretical method, the run time statistics, to study analytically quenched growth models. Those models are characterized by quenched noise and extremal statistics.

The application of this method, together with other tools such as the FST [20] or the real space RG [10], allows us to get very good estimations for the scaling exponents. Here we have considered explicitly the cases of invasion percolation and directed invasion percolation, to which we applied the FST technique [7] to obtain the fractal dimension D_f of the clusters of IP, IP with trapping, and DIP. In particular, nonlocal effects like that of trapping, which poses insurmountable difficulties to other approaches, can be dealt with in a remarkably accurate way. The results of the FST calculation, apart from the case of site trapping (and for reasons which are easily understood), all display a remarkable accuracy: the deviation from the accepted result being at most 0.5%. The present approach therefore provides a first principle analytical framework to understand self-organization and to compute the various critical exponents for the extremal problems.

In addition, we have shown that the scale-invariant dynamics allows us to evaluate also the avalanche size distribution exponent τ that we computed in detail for the case of IP. This method could in principle be applied also to the computation of the avalanche exponent of DIP, but at the moment we have to solve some problems related to the peculiar, asymmetric distribution of boundary conditions of DIP.

The theoretical methods presented in this paper open two research directions. From one side a deeper understanding of the mathematical properties of the RTS would be most welcome. As we have shown, the RTS provides only an approximation on the statistical weight of quenched processes. The main question concerns whether or not the error in this *intrinsic* approximation becomes negligible as the length of the process increases. In the affirmative case, one would also like to have a control on the magnitude of this error. We are actively investigating this problem [8,13]. Another interesting problem is to see if it is possible to define the RTS for quenched dynamics different from the extremal dynamics. A step forward for ''equilibrium'' disordered systems has been recently made [29].

On the other hand, one can extend the RTS approach to other models such as surface dynamics with quenched disorder, where the extremal dynamics is combined with surface tension effects [5], or to models where the quenched disorder is coupled to a spatial field. The prototype of the latter situation is quenched DBM (QDBM) [2,3], where the extremal dynamics applies to a combination of the disorder field (which acts as a random threshold) and the electric field. The main interest in such a model lies in the fact that phenomena like fracture propagation in crystals are conditioned both by quenched factors (defects and microcracks) and by time-dependent factors (electric fields, strain). Significant progress, which we plan to present in the future, has also been made in this direction.

APPENDIX A: DERIVATION OF THE RTS EQUATIONS

In this appendix we compute explicitly the expressions (7)–(9). Let us recall some properties of a set of continuous independent random variables. Given a set of variables $\{X_1, X_2, \ldots, X_N\}$ and their probability densities $\{p_1(x_1), p_2(x_2), \ldots, p_N(x_N)\}$, we fix an order relation such as, for example, $X_1 < X_2 < \cdots < X_N$. The probabilities to have such an ordering between the variables are

$$\text{Prob}[(x_1 \leq X_1 \leq x_1 + dx_1) \cap (X_1 < X_2 < \cdots < X_N)]$$

$$= dx_1 p_1(x_1) \int_{x_1}^{1} dx_2 p_2(x_2) \cdots \int_{x_{N-1}}^{1} dx_N p_N(x_N) \tag{A1}$$

for $X_1 \in [x, x+dx]$ and

$$\text{Prob}(X_1 < X_2 < \cdots < X_N)$$

$$= \int_0^1 \text{Prob}[(x_1 \leq X_1 \leq x_1 + dx_1) \cap (X_1 < X_2 < \cdots < X_N)] \tag{A2}$$

for $X_1 \in [0,1]$. Equation (A1) expresses the effective density for the variable X_1 conditional to the given order relation, while Eq. (A2) is the total probability to have the order relation $X_1 < X_2 < \cdots < X_N$.

Using Eqs. (A1) and (A2) we can compute the following probability:

$$\text{Prob}[(x_1 \leqslant X_1 \leqslant x_1 + dx_1) \cap (X_1 = \min_{m=l,\ldots N} X_m)]$$

$$= dx_1 p_1(x_1) \sum_{\{p_2,\ldots,p_N\}} \left[\int_{x_1}^{1} dx_{p_2} p_{p_2}(x_{p_2}) \cdots \right.$$

$$\left. \times \int_{x_{p_{N-1}}}^{1} dx_{p_N} p_{p_N}(x_{p_N}) \right], \tag{A3}$$

where the sum is over all permutations of the ordered set $\{2,\ldots,N\}$ and

$$\text{Prob}(x_1 = \min_{m=1,\ldots,N} X_m)$$

$$= \int_{x_1=0}^{x_1=1} \text{Prob}[(x_1 \leqslant X_1 \leqslant x_1 + dx_1)$$

$$\cap (X_1 = \min_{m=1,\ldots,N} X_m)]. \tag{A4}$$

Equation (A3) represents the probability that the variable X_1, with value ranging between x and $x+dx$, is the smallest in the set, independently of the ordering of the others. Equation (A4) is instead the probability that X_1 will be the minimum one irrespective of its value. At this point one can demonstrate by induction that

$$\sum_{\{p_2,\ldots,p_N\}} \left[\int_{x_1}^{1} dx_{p_2} p_{p_2}(x_{p_2}) \cdots \int_{x_{p_{N-1}}}^{1} dx_{p_N} p_{p_N}(x_{p_N}) \right]$$

$$= \prod_{m=2}^{N} \int_{x_1}^{1} dx_m p_m(x_m). \tag{A5}$$

The result of Eq. (A5) may appear trivial. However, in more complex cases it is important to keep the formalism general.

Introducing Eq. (A5) into Eqs. (A3) and (A4) one gets

$$\text{Prob}[(x_1 \leqslant X_1 \leqslant x_1 + dx_1) \cap (X_1 = \min_{m=1,\ldots,N} X_m)]$$

$$= dx_1 p_1(x_1) \prod_{m=2}^{N} \int_{x_1}^{1} dx_m p_m(x_m) \tag{A6}$$

and

$$\text{Prob}(X_1 = \min_{m=1,\ldots,N} X_m)$$

$$= \int_0^1 dx_1 p_1(x_1) \prod_{m=2}^{N} \int_{x_1}^{1} dx_m p_m(x_m). \tag{A7}$$

In invasion percolation a bond grows at time t if its variable is the minimum one at that time. So, using Eq. (A6) we can write

$$\text{Prob}(t; (x \leqslant \epsilon_i \leqslant x + dx)(\epsilon_i = \min_{m \in \partial \mathcal{C}_t} \epsilon_m))$$

$$= dx \rho_{i,t}(x) \prod_{m \in \partial \mathcal{C}_t - \{i\}} \int_x^1 \rho_{m,t}(y) dy \tag{A8}$$

or, in terms of the $p_{k,t}(x)$,

$$\text{Prob}(t; (x \leqslant \epsilon_i \leqslant x + dx) \cap (\epsilon_i = \min_{m \in \partial \mathcal{C}_t} \epsilon_m))$$

$$= dx\ p_{k,t}(x) \prod_{\theta} [1 - P_{\theta,t}(x)]^{n_{\theta,t} - \delta_{\theta,k}}, \tag{A9}$$

where $P_{\theta,t}(x) = \int_0^x dy p_{\theta,t}(y)$ and the Kronecker delta means that the product is over all the variables but the growing one.

Integrating Eq. (A9) one can finally write the growth probability $\mu_{k,t}$ for the bond i at time t [8]:

$$\mu_{k,t} \equiv \text{Prob}(t; \epsilon_i = \min_{m \in \partial \mathcal{C}_t} \epsilon_m)$$

$$= \int_0^1 dx p_{k,t}(x) \prod_{\theta} [1 - P_{\theta,t}(x)]^{n_{\theta,t} - \delta_{\theta,k}}. \tag{A10}$$

For the computation of the density of the smallest random variable $m_{k,t}(x)$ *after* it has grown we use the rule of conditional probability, which we recall here:

$$\text{Prob}(A|B) = \frac{\text{Prob}(A \cap B)}{\text{Prob}(B)}, \tag{A11}$$

where $A \equiv (x \leqslant \epsilon_i \leqslant x + dx)$ and $B \equiv (\epsilon_i = \min_{m \in \partial \mathcal{C}_t} \epsilon_m)$. One has

$$m_{k,t}(x) dx \equiv \text{Prob}(t; (x \leqslant \epsilon_i \leqslant x + dx) | (\epsilon_i = \min_{m \in \partial \mathcal{C}_t} \epsilon_m))$$

$$= \frac{\text{Prob}(t; (x \leqslant \epsilon_i \leqslant x + dx) \cap (\epsilon_i = \min_{m \in \partial \mathcal{C}_t} \epsilon_m))}{\text{Prob}(t; \epsilon_i = \min_{m \in \partial \mathcal{C}_t} \epsilon_m)}$$

$$= \left(dx p_{k,t}(x) \prod_{\theta} [1 - P_{\theta,t}(x)]^{n_{\theta,t} - \delta_{\theta,k}} \right) 2 \mu_{k,t} \tag{A12}$$

and finally

$$m_{k,t}(x) = \frac{p_{k,t}(x) \prod_{\theta} [1 - P_{\theta,t}(x)]^{n_{\theta,t} - \delta_{\theta,k}}}{\mu_{k,t}}. \tag{A13}$$

In the same way we can calculate the effective densities of the ''surviving'' perimeter bonds $\rho_{i,t+1}(x) \equiv p_{\theta+1,t+1}(x)$, where the events A and B are, respectively, $A \equiv (x \leqslant \epsilon_j \leqslant x + dx)$ and $B \equiv (\epsilon_i = \min_{m \in \partial \mathcal{C}_t} \epsilon_m)$:

$$\text{Prob}(t+1; x \leqslant \epsilon_j \leqslant x + dx) = dx p_{\theta+1,t+1}(x) \equiv dx \rho_{j,t+1}(x). \tag{A14}$$

But,

$$\text{Prob}(t+1; x \leqslant \epsilon_j \leqslant x + dx)$$

$$= \text{Prob}(t; (x \leqslant \epsilon_j \leqslant x + dx) | (\epsilon_i = \min_{m \in \partial \mathcal{C}_t} \epsilon_m))$$

$$= \frac{\text{Prob}(t; (x \leqslant \epsilon_j \leqslant x + dx) \cap (\epsilon_i = \min_{m \in \partial \mathcal{C}_t} \epsilon_m))}{\text{Prob}(t; \epsilon_i = \min_{m \in \partial \mathcal{C}_t} \epsilon_m)}. \tag{A15}$$

The numerator of (64) can be written as

$$\begin{aligned}&\mathrm{Prob}(t;(x\leqslant\epsilon_j\leqslant x+dx)\cap(\epsilon_i=\min_{m\in\partial\mathcal{C}_t}\epsilon_m))\\&=dx\ \rho_{j,t}(x)\int_0^x dy\rho_{i,t}(y)\prod_{m\in\partial\mathcal{C}_t-\{i,j\}}\left(\int_y^1 du\rho_{m,t}(u)\right)\\&\equiv dx p_{\theta,t}(x)\int_0^x dy\left[p_{k,t}(y)\prod_\zeta\left[1-P_{\zeta,t}(y)\right]^{n_{\zeta,t}-\delta_{\zeta,k}-\delta_{\zeta,\theta}}\right]\end{aligned}\tag{A16}$$

while the denominator is $\mu_{k,t}$. So we have

$$\begin{aligned}p_{\theta+1,t+1}(x)=\frac{1}{\mu_{k,t}}\Bigg[p_{\theta,t}(x)\int_0^x dy\Bigg(p_{k,t}(y)\\\times\prod_\zeta\left[1-P_{\zeta,t}(y)\right]^{n_{\zeta,t}-\delta_{\zeta,k}-\delta_{\zeta,\theta}}\Bigg)\Bigg].\end{aligned}\tag{A17}$$

Or, using (8):

$$p_{\theta+1,t+1}(x)=p_{\theta,t}(x)\int_0^x\frac{m_{k,t}(y)}{[1-P_{\theta,t}(y)]}dy.\tag{A18}$$

APPENDIX B: VOID DISTRIBUTION FOR AN ANISOTROPIC RANDOM CANTOR SET

In this appendix we derive the expression for the void distribution $P(\lambda=0)$ of an anisotropic random Cantor set in terms of the C_i.

As for the isotropic case [29] we start from the system at the biggest scale, coinciding with a single occupied unitary cell of length L, and proceed to a fragmentation into two consecutive cells with probability distribution given by the weights C_0,C_1,C_2 (Fig. 13), with the conditions

$$\begin{aligned}&C_0+C_1+C_2=1,\\&C_i>0\quad\text{for}\quad i=1,2,3.\end{aligned}\tag{B1}$$

After n steps of fragmentation the unitary cell will have a length $(1/2)^n\times L$. For the sake of simplicity we fix $L=1$. Now we measure the voids after n iterations in units of $(1/2)^n$. Let us call $N_l^{(n)}$ the number of clusters of points of length l after n iterations and $V_l^{(n)}$ the number of voids of length l. The quantity we have to compute is the conditional probability $P(\lambda)$ that, given an occupied unitary cell, it has at its left (or right) side a void of length l. Even if we have asymmetric generators, we will see that $P(\lambda)$ is the same for left-hand and right-hand voids.

Because of the self-similarity of the Cantor set one has [29]

$$P(\lambda)=\lim_{n\to\infty}\frac{V_\lambda^{(n)}}{\sum_{l=1}^{\infty}lN_l^{(n)}}.\tag{B2}$$

We are interested only in $P(\lambda=0)$, that is, the probability that given an occupied unitary cell it is followed by another occupied cell. One can show that [29]

$$P(\lambda=0)=\lim_{n\to\infty}\frac{\sum_l(l-1)N_l^{(n)}}{\sum_l lN_l^{(n)}}=1-\lim_{n\to\infty}\frac{\sum_l N_l^{(n)}}{\sum_l lN_l^{(n)}}.\tag{B3}$$

Until now our discussion is valid for both the isotropic and the anisotropic case. Now we proceed to compute the limit in Eq. (B3).

The denominator of the fraction in Eq. (B3) can be written as

$$\begin{aligned}\sum_l lN_l^{(n+1)}&=(C_0+C_1)\sum_l lN_l^{(n)}+2C_2\sum_l lN_l^{(n)}\\&=(1+C_2)\sum_l lN_l^{(n)},\end{aligned}\tag{B4}$$

where the last member of Eq. (B4) is due to the first relation in (B1). This expression is clearly invariant under the exchange of C_0 with C_1 and vice versa.

So, we get the same expression for left and right voids. The numerator of the fraction in the last member is instead, for right-hand voids,

$$\sum_l N_l^{(n+1)}=\sum_l N_l^{(n)}[1+(l-1)C_1+(l-1)C_0(C_0+C_2)].\tag{B5}$$

The corresponding expression for left-hand voids is

$$\sum_l N_l^{(n+1)}=\sum_l N_l^{(n)}[1+(l-1)C_0+(l-1)C_1(C_1+C_2)].\tag{B6}$$

Because of the condition $C_0+C_1+C_2=1$ Eqs. (B5) and (B6) coincide.

Introducing $C_0=1-C_1-C_2$ in Eq. (B5),

$$\begin{aligned}\sum_l N_l^{(n+1)}=\sum_l N_l^{(n)}[1+(l-1)(1-C_1-C_2+C_1C_2\\+C_1^2)].\end{aligned}\tag{B7}$$

So, we have

$$\begin{aligned}\frac{\sum_l N_l^{(n+1)}}{\sum_l lN_l^{(n+1)}}&=\frac{1-C_1-C_2+C_1C_2+C_1^2}{1+C_2}\\&\quad+\frac{C_1+C_2-C_1C_2-C_1^2}{1+C_2}\frac{\sum_l N_l^{(n)}}{\sum_l lN_l^{(n)}}.\end{aligned}\tag{B8}$$

Taking the limit $n\to\infty$ for both sides of Eq. (B8) we obtain

$$P(\lambda=0)=\frac{C_2}{1-C_1+C_1C_2+C_1^2}. \tag{B9}$$

Equation (B9) can be used in the FST calculations for DIP.

We have to solve the following system [29,6,7]:

$$\begin{pmatrix} C_0 \\ C_1 \\ C_2 \end{pmatrix} = \begin{pmatrix} M_{0,0} & M_{1,0} & M_{2,0} \\ M_{0,1} & M_{1,1} & M_{2,1} \\ M_{0,2} & M_{1,2} & M_{2,2} \end{pmatrix} \begin{pmatrix} C_0 \\ C_1 \\ C_2 \end{pmatrix}, \tag{B10}$$

with the conditions (B1) and $\Sigma_{j=1}^{3}M_{i,j}=1$ for $i=1,2,3$. The three equations in (B10) are not independent. We can drop one of them and use the normalization condition for the C_i. From the dynamical DIP′s rules one infers that, independently from the boundary conditions, one has $M_{1,0}=M_{0,1}=0$ and in open conditions one has also $M_{0,2}^{\rm op}=1$ (this is a manifestation of the asymmetry of the model).

The expression for the FST matrix elements in the open-closed approximation is [6,7]:

$$M_{i,j}=P(\lambda=0)M_{i,j}^{\rm cl}+[1-P(\lambda=0)]M_{i,j}^{\rm op}, \tag{B11}$$

where $P(\lambda=0)$ is given by (B9). If we introduce Eqs. (B11), (B9) into the linear system (B10) we obtain a nonlinear system in C_i. Such a system admits the trivial solution $C_0=1$ and $C_1=C_2=0$. This solution cannot be accepted in view of the conditions (B1) for C_i. The other solutions are given by the system

$$\begin{aligned} &-M_{1,2}^{\rm op}(C_1-C_1^2+C_1^3)+\frac{1-M_{2,0}^{\rm op}-M_{0,0}^{\rm cl}+(M_{0,0}^{\rm cl}+M_{2,0}^{\rm op}-1)C_1-M_{2,0}^{\rm op}C_1^2}{1+M_{2,0}^{\rm cl}-M_{2,0}^{\rm op}-M_{0,0}^{\rm cl}+M_{2,0}^{\rm op}C_1}\Bigg(M_{2,1}^{\rm op}+(M_{1,2}^{\rm op}-M_{1,2}^{\rm cl}-M_{2,1}^{\rm op})C_1+(M_{2,1}^{\rm op}-M_{1,2}^{\rm op})C_1^2 \\ &+(M_{2,1}^{\rm cl}-M_{2,1}^{\rm op}+M_{2,1}^{\rm op})C_1\frac{1-M_{2,0}^{\rm op}-M_{0,0}^{\rm cl}+(M_{0,0}^{\rm cl}+M_{2,0}^{\rm op}-1)C_1-M_{2,0}^{\rm op}C_1^2}{1+M_{2,0}^{\rm cl}-M_{2,0}^{\rm op}-M_{0,0}^{\rm cl}+M_{2,0}^{\rm op}C_1}\Bigg)=0, \end{aligned} \tag{B12}$$

$$C_2=\frac{1-M_{2,0}^{\rm op}-M_{0,0}^{\rm cl}+(M_{0,0}^{\rm cl}+M_{2,0}^{\rm op}-1)C_1-M_{2,0}^{\rm op}C_1^2}{1+M_{2,0}^{\rm cl}-M_{2,0}^{\rm op}-M_{0,0}^{\rm cl}+M_{2,0}^{\rm op}C_1}.$$

The first equation cannot be solved analytically. We solved it using the Newton's contractions method and accepting only the solutions satisfying the constraint $C_i>0$. The solution of the system (B12) leads to the results of Table I [31,32].

[1] D. Wilkinson and J. F. Willemsen, J. Phys. A **16**, 3365 (1983).
[2] L. De Arcangelis, A. Hansen, H. J. Herrmann, and S. Roux, Phys. Rev. B **40**, 877 (1989); F. Family, Y. C. Zhang, and T. Vicsek, J. Phys. A **19**, L733 (1986).
[3] A. Hansen, E. L. Hinrichsen, S. Roux, H. J. Herrmann, and L. De Arcangelis, Europhys. Lett. **13**, 341 (1990).
[4] P. Bak and K. Sneppen, Phys. Rev. Lett. **71**, 4083 (1993); for a general discussion see P. Bak, M. Paczusky, and S. Maslov, Phys. Rev. E **53**, 414 (1996).
[5] K. Sneppen, Phys. Rev. Lett. **69**, 3539 (1992).
[6] L. Pietronero, A. Erzan, and C. Evertsz, Phys. Rev. Lett. **61**, 861 (1988); Physica A **151**, 207 (1988).
[7] A. Erzan, L. Pietronero, and A. Vespignani, Rev. Mod. Phys. **67**, 545 (1995).
[8] M. Marsili, J. Stat. Phys. **77**, 733 (1994).
[9] L. Pietronero, W. R. Schneider, and A. Stella, Phys. Rev. A **42**, R7496 (1990); L. Pietronero and W. R. Schneider, Physica A **119**, 249 (1990).
[10] M. Marsili, Europhys. Lett. **28**, 385 (1994).
[11] S. Roux and E. Guyon, J. Phys. A **22**, 3693 (1989).
[12] S. Maslov, Phys. Rev. Lett. **74**, 562 (1995).
[13] M. Marsili, R. Cafiero, and A. Gabrielli (unpublished).
[14] A. Gabrielli, M. Marsili, R. Cafiero, and L. Pietronero, J. Stat. Phys. (to be published).
[15] D. Stauffer and A. Aharony, *Introduction to Percolation Theory* (Taylor & Francis, London, 1985).
[16] R. Chandler, J. Koplik, K. Lerman, and J. F. Willemsen, J. Fluid Mech. **119**, 249 (1982).
[17] R. Lenormand and R. Bories, C. R. Acad. Sci. **291**, 279 (1980).
[18] J. T. Chayes, L. Chayes, and C. M. Newmann, Commun. Math. Phys. **101**, 383 (1985); **101**, 285 (1985).
[19] L. Niemeyer, L. Pietronero, and H. J. Wiesmann, Phys. Rev. Lett. **52**, 1033 (1984).
[20] R. De Angelis, M. Marsili, L. Pietronero, A. Vespignani, and H. J. Wiesmann, Europhys. Lett. **16**, 417 (1991).
[21] R. Cafiero, L. Pietronero, and A. Vespignani, Phys. Rev. Lett. **70**, 3939 (1993).
[22] M. Marsili, G. Caldarelli, and M. Vendruscolo, Phys. Rev. E **53**, 13 (1996).
[23] B. Mandelbrot, J. Fluid. Mech. **62**, 331 (1974).
[24] A. P. Siebesma, Ph.D. thesis, The CheesePress, Edam, The Netherlands, 1989.
[25] A. Vespignani and L. Pietronero, Physica A **168**, 723 (1990)
[26] W. Kinzel, Ann. Israel Phys. Soc. **5**, 425 (1983).
[27] R. Baxter and A. J. Guttman, J. Phys. A **xx**, 3193 (1988).
[28] R. R. Tremblay and A. P. Siebesma, Phys. Rev. A **40**, 5377 (1989).
[29] M. Vendruscolo and M. Marsili (unpublished).